

Anhyseretic remanent magnetization of fine magnetic particles

R. Egli and W. Lowrie

Institute of Geophysics, ETH Hnggerberg, Zrich, Switzerland

Received 15 June 2001; revised 25 January 2002; accepted 30 January 2002; published 3 October 2002.

[1] Various magnetic parameters are in common use for estimating the grain size of magnetic particles. Among these, the ratio of the intensity of anhysteretic remanent magnetization (ARM) to that of isothermal remanent magnetization, as well as their alternating field (AF) demagnetization curves are used as an indicator of the domain state of the particles. Several models have been proposed to describe physically the acquisition of ARM in a biased AF field. *Jaep* [1969] first developed a semiquantitative theory based entirely on the thermal fluctuation analysis developed by *Nel* [1949, 1954, 1955]. Significant discrepancies were found between his model and experimental results on magnetite. A new, general theory of ARM based on the work of *Jaep* is presented here, with particular regard to the influence of various parameters like grain size, coercivity, and mineralogy on ARM intensity. An analytical expression for ARM intensity in the special case of very fine particles was derived from this theory, and a good agreement with experimental results and data from the literature was found. A new estimation of the atomic reorganization time was obtained from ARM measurements on a sample of the Yucca Mountain Tuff, which has well-known mineralogy and grain-size distribution. The results are in agreement with the value proposed by *McNab et al.* [1968] for magnetite. Some authors considered magnetic interactions as the key to understand the ARM in fine particles, and this is certainly true for strongly interacting samples. In this case, ARM would be useless for the characterization of magnetic grains. However, many sediments have a very low concentration of well-distributed magnetic grains. For these samples, the explanation of an ARM in terms of intrinsic properties of the grains, as qualitatively proposed by other authors, is more suitable. **INDEX TERMS:** 1540 Geomagnetism and Paleomagnetism: Rock and mineral magnetism; 1512 Geomagnetism and Paleomagnetism: Environmental magnetism; **KEYWORDS:** thermal fluctuations, ARM, single domain, coercivity, Lowrie-Fuller test

Citation: Egli, R., and W. Lowrie, Anhysteretic remanent magnetization of fine magnetic particles, *J. Geophys. Res.*, 107(B10), 2209, doi:10.1029/2001JB000671, 2002.

1. Introduction

[2] In studies of environmental magnetism the variations in grain size are conveniently described by magnetic parameters. Among these, it is common to use the ratio of anhysteretic remanent magnetization (ARM) to bulk susceptibility or to isothermal remanent magnetization (IRM). Interpretation of variations in these parameters is inhibited by lack of fundamental theoretical understanding of how they relate to grain size. The interpretation of many magnetic profiles in sediments is largely empirical, based upon experimental observations made on sized fractions of selected magnetic minerals. A comparison between the demagnetization characteristics of ARM and IRM was proposed as a discriminant between single domain (SD) and multidomain (MD) carriers of remanence [*Johnson et al.*, 1975]. However, an adequate theory of ARM has not yet been developed. In this paper we address the theory of ARM in SD particles.

[3] Several theoretical studies have been made of ARM in fine particles, because of its importance in the recording process on magnetic tapes [*Wohlfarth*, 1964; *Jaep*, 1969]. Assuming ARM as a proxy for TRM, *Bailey and Dunlop* [1977] proposed its application in paleointensity determinations as a nondestructive alternative.

[4] In a series of studies [*Wohlfarth*, 1964; *Kneller*, 1968] of ARM in SD particles the classical Stoner-Wohlfarth theory [*Stoner and Wohlfarth*, 1948] was used. This theory ignores the effect of thermal energy fluctuations on the magnetic moment of the particles. It predicts an infinite susceptibility of ARM for noninteracting SD particles. However, experimental values are finite, and to account for this, the effect of magnetic interactions between the particles was introduced [*Wohlfarth*, 1964; *Dunlop and West*, 1969]. Consequently, *Kneller* [1968] proposed that ARM measurements could be used to study the interaction fields. *Eldridge* [1961] showed that intuitive interaction models, which assume the mean interaction field to be proportional to the magnetization [*Nel*, 1954], fail to predict a finite susceptibility of ARM. In order to explain the finite susceptibility of ARM in SD particles

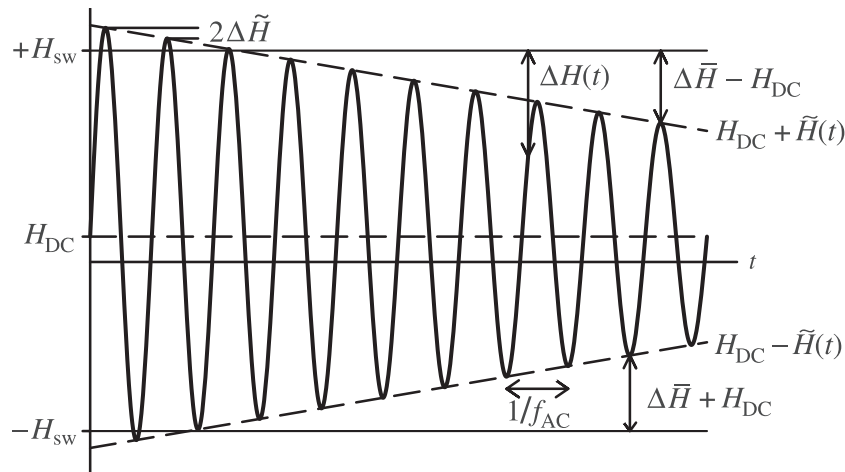


Figure 1. The applied field during an ARM cycle. Notations are explained in the text.

more complex interaction models, based on the Preisach-Néel theory were developed [Wohlfarth, 1964; Dunlop and West, 1969].

[5] These models do not take into account thermodynamic effects. The theory of thermoremanent magnetization (TRM) and its coercivity parameters in single-domain particles depends strongly on the concept of a fluctuation field, which was first introduced by Néel [1955] and later utilized by Dunlop [1965] and Kneller and Wohlfarth [1966]. The fluctuation field is a key factor in explaining the dependence of coercivity parameters on temperature, particle volume and time. For example, it allowed Kneller and Wohlfarth [1966] to predict how ARM intensity varies with the temperature of acquisition.

[6] The approach to the problem of thermodynamic effects on the magnetization of SD particles is based on the thermal fluctuation analysis of Néel [1949]. Several later studies based on more general physical models of thermally induced activation processes resulted in improved versions of the Néel theory [Brown, 1959, 1963] but for practical purposes lead to substantially the same results [Brown, 1959].

[7] Jaep [1969] first proposed a semiquantitative model for ARM in SD particles, based entirely on thermal fluctuation analysis, which predicts a finite ARM susceptibility even in the noninteracting case. According to this model, thermodynamic fluctuation theory is not merely an additional factor which affects ARM, it is the key mechanism in understanding the acquisition process. Later, Jaep evaluated the effect of magnetic interactions in his thermodynamic model, focusing on materials used for magnetic tapes. In these materials interactions play a major role because of the high volume concentration of magnetic particles [Jaep, 1971].

[8] This paper presents a strictly quantitative theory of ARM acquisition in SD particles. On the basis of Jaep's approach and on the thermal fluctuation analysis of Néel, it demonstrates that the intensity of ARM is strongly controlled by thermodynamic conditions. The theory is extended to alternating field (AF) demagnetization and includes calculation of the fluctuation field. Finally, measurements on natural samples are presented as an exper-

imental confirmation of the theory. The possible results of the modified Lowrie-Fuller test [Johnson *et al.*, 1975] for noninteracting SD particles with different volume and microcoercivity distributions are also discussed.

2. ARM Acquisition Without Thermal Activation

[9] In this paper the following notations will be used for the alternating (AC) and direct (DC) field components (Figure 1):

| | |
|-------------------|---|
| H_{DC} | DC field, superimposed on the AC field; |
| \tilde{H} | amplitude of the AC field; |
| \tilde{H}_0 | maximum amplitude of the AC field; |
| f_{AC} | frequency of the AC field; |
| $\Delta\tilde{H}$ | decay rate of the AC field in field units per half cycle. |

Common values in real ARM experiments are $H_{DC} = 0.1 - 1$ mT, $\tilde{H}_0 \geq 10 - 300$ mT, $f_{AC} = 50 - 400$ Hz, $\Delta\tilde{H} = 1..10$ μ T/half cycle. In the following calculations we assume $H_{DC} > \Delta\tilde{H}$, which is generally valid in real ARM experiments.

[10] Consider the acquisition of ARM by a uniaxial SD particle in an assemblage of noninteracting grains. We model the behavior of this particle in a magnetic field H with the Stoner-Wohlfarth theory [Stoner and Wohlfarth, 1948]. Assume that its magnetization is homogeneous and that it defines an angle θ with the easy axis, which in turn defines an angle φ with the applied field H , as in Figure 2.

[11] Let $m = M_s V$ be the magnetic moment of the particle with volume V and saturation magnetization M_s , and let H_K be its microcoercivity. The free energy E of this particle in a field H is given by

$$E/E_0 = \sin^2 \theta - 2h \cos(\varphi - \theta) \quad (1)$$

with $E_0 = \mu_0 m H_K / 2$ and $h = H/H_K$. Let $\varepsilon = E/E_0$ be the reduced free energy. At equilibrium, θ defines a local minimum in ε , according to the conditions $\partial\varepsilon/\partial\theta = 0$ and $\partial^2\varepsilon/\partial\theta^2 < 0$ for the orientation of m . Note that in the Stoner-Wohlfarth model expressed in equation (1), the thermal energy kT is neglected. The magnetic moment

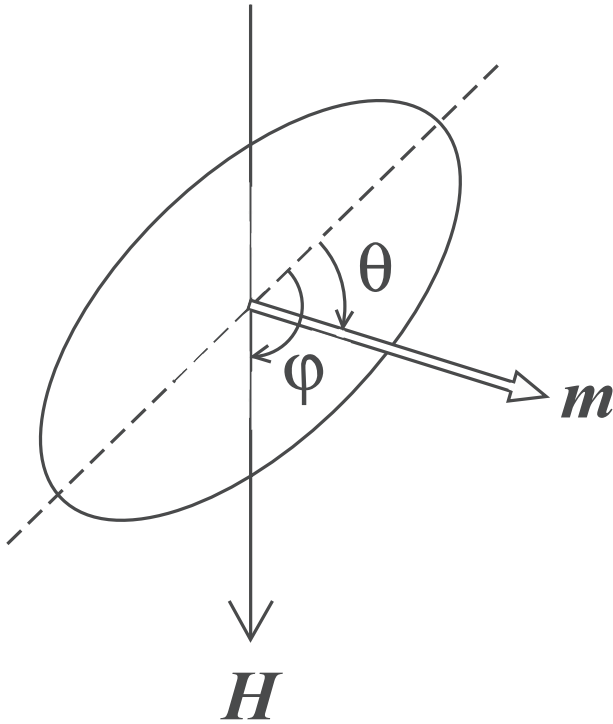


Figure 2. The magnetization of a SD particle in the Stoner-Wolfarth model. The dashed line indicates the easy axis of the particle.

component m_{\parallel} parallel to the applied field gives a hysteresis loop. The absolute value of the field H_{sw} at which m_{\parallel} is discontinuous and changes sign will be called the switching field. The shape of the hysteresis loop and the value of H_{sw} depend on φ . Some examples are given by *Dunlop and Özdemir* [1997].

[12] At $H = H_{sw}$ the local minima of equation (1) disappears, and $\partial^2\epsilon/\partial\theta^2 = 0$, with following solution:

$$h_{sw} = \frac{\sqrt{1-t^2+t^4}}{1+t^2}, \quad t = \tan^{1/3}\varphi, \quad (2)$$

$$\tan \theta_{sw} = \frac{\sqrt{3} - \sqrt{4h_{sw}^2 - 1}}{2\sqrt{1-h_{sw}^2}}$$

where $h_{sw} = H_{sw}/H_K$ and θ_{sw} is the value of θ at which switching occurs [*Stoner and Wohlfarth*, 1948]. In general, $0.5 < h_{sw} < 1$.

[13] We consider now the behavior of such a SD particle with switching field H_{sw} during an ARM represented in Figure 3a. The arrows represent the direction of m_{\parallel} , parallel (upward arrow) or antiparallel (downward arrow) to the applied DC field. If $H_{sw} < \dot{H}_0$, m_{\parallel} is always parallel to the applied DC field at the end of the ARM acquisition, independently of the initial state of the particle. Extending the model to all particles with different switching fields, we conclude that all particles with $H_{sw} \leq \dot{H}_0$ are reoriented with a positive m_{\parallel} during the ARM.

[14] According to this model, the ARM acquired by all the particles is identical to an IRM given in a DC field equal to \dot{H}_0 . However, it is well known experimentally that ARM intensities are always a fraction of the IRM, even for an assembly of SD noninteracting particles. Moreover, according to this model the ARM intensity is independent of H_{DC} , and gives an infinite ARM susceptibility, in contradiction of experimental observations.

3. ARM Acquisition With Thermal Activation

[15] We extend now the model of section 1 in order to take into account the thermal energy kT of the particles, and develop the kinetic equations for SD particles in a biased AC field.

3.1. Previous Studies

[16] *Néel* [1949] developed the kinetic equations for an array of aligned noninteracting particles, in order to model thermoremanent magnetization. *Jaep* [1969] applied the work of *Néel* to anhysteretic magnetization processes.

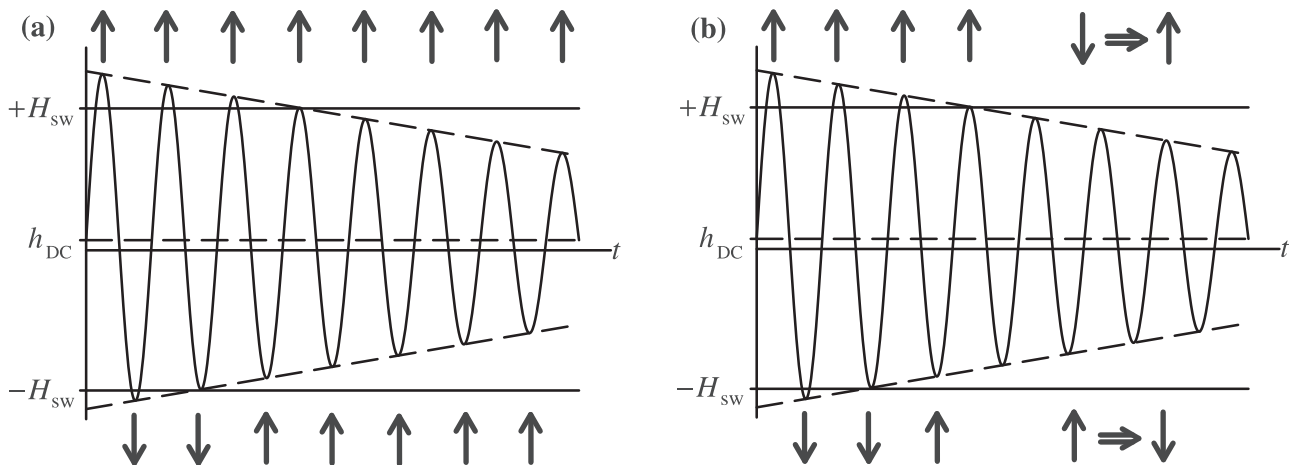


Figure 3. Magnetic moment of a particle during an ARM cycle (a) according to the Stoner-Wolfarth model and (b) according to a thermodynamic model. Arrows represent the direction of the magnetic moment parallel (upward arrow) or antiparallel (downward) to the DC field. In Figure 3a the moment is frozen-in once the amplitude of the AC field becomes smaller than the switching field. In Figure 3b, thermodynamically activated switching events occur when the AC field is smaller than the switching field.

Later he introduced the effect of magnetic interactions through the thermodynamic formalism and obtained the following expression for the acquisition of ARM by aligned interacting particles:

$$\frac{M}{M_{rs}} = \tanh \left[\frac{\mu_0 m}{kT} (\beta H_{DC} - \lambda M/M_{rs}) \right] \quad (3)$$

$$\beta = \frac{(M_s)_B}{M_s} \left(\frac{T}{T_B} \right)^{1/2} \leq 1$$

where M_s is the saturation magnetization, M_{rs} is the saturation of remanence, T is the absolute temperature and $(M_s)_B$ is the saturation magnetization at the blocking temperature T_B of the particles. The parameter λ is a measure of the average interaction field. Equation (3) predicts a finite susceptibility of ARM even in the noninteracting case, but is independent of the characteristics of the AC field (i.e., its frequency f_{AC} and its decay rate per half cycle $\Delta\tilde{H}$).

[17] Most studies of thermal activation in SD particles assumed an alignment between applied field and easy axis of the particles, to reduce the mathematical complexity of the models used. However, in a set of randomly oriented particles, only a negligible part of them satisfy this condition. *Victoria* [1989] pointed out that the energy barrier for randomly oriented particles exhibits a 3/2 power dependence on the applied field, in contrast to the quadratic dependence for aligned particles. This may introduce significant differences in modeling relaxation processes.

[18] *Walton* [1990] introduced a new approach to the problem, trying to partially solve the kinetic equations for noninteracting SD particles in an AC field. He also extended his calculations to the more general case of a particle whose easy axis defines an angle φ with the applied field, and obtained the following expression for the susceptibility of ARM:

$$\chi_{ARM}(\varphi) = \mu_0 \frac{2r}{3\mu_0 q(\varphi) H_K} \left(\frac{\mu_0 m H_K}{2kT} \right)^{1/r} \ln^{1-1/r} \left[\frac{F_0}{2\pi f_{AC}} \left(\frac{2kT}{\mu_0 m H_K} \right)^{3/2} \right] \quad (4)$$

where $1 \leq q \leq 2$ and $1.5 \leq r \leq 2$ are functions of φ , and $F_0 \approx 10^9$ Hz is the frequency of the thermal activations. Because of the presence of r as exponent in equation (4), it is impossible to generalize this expression for the case of an assembly of randomly oriented particles. However, equation (4) with $r = 1.5$ (and $\varphi = \pi/4$) is very similar to the result of this paper, given by (32) for randomly oriented particles. Equation (4) shows a weak dependence on f_{AC} but curiously no dependence on $\Delta\tilde{H}$. This may be a consequence of some approximations adopted to simplify the calculations.

[19] The results mentioned above are all based on some simplifications which reduce their general validity. For this reason, we here apply the thermal relaxation theory to the most general case of a set of noninteracting randomly oriented particles and solve directly the resulting kinetic equations. A similar result to equation (4) is obtained for the anhysteretic magnetization. However, a well-defined dependence on the moment m , the temperature T , and the microcoercivity H_K is found. In addition, our result shows

a weak dependence on both frequency and ramp rate of the AC field used for the ARM.

3.2. Derivation of the Field-Antiparallel Switching Frequency

[20] We consider again the moment of a particle in the ARM field, as represented in Figure 3. At a given point, when the AC peak field becomes smaller than H_{sw} , the particle moment is “frozen” in a stable position (a local minimum of ϵ). For several cycles, the applied field reaches values very near to H_{sw} . The energy barrier represented by the difference between the local maximum and minimum is reduced to small values, of the same order of magnitude as the thermal energy.

[21] According to Figure 1, we define

$$\begin{aligned} H(t) &= H_{DC} + \bar{H}(t) \cos(2\pi f_{AC} t) \\ \Delta H(t) &= |H_{sw} - \bar{H}(t) \cos(2\pi f_{AC} t)| \\ \Delta \bar{H}(t) &= |H_{sw} - \bar{H}(t)| \end{aligned} \quad (5)$$

$H(t)$ is the total applied field at instant t during the ARM acquisition. It is the sum of the constant bias field H_{DC} and the amplitude of the alternating field at time t . The energy barrier ΔE to overcome a local minimum in E is a function of ΔH , namely, $\Delta E = \Delta E(\Delta H)$; in particular, $\Delta E = 0$ when $\Delta H = 0$. In this situation, if ΔH is small enough, thermally activated switching of m is possible. The frequency of switching is given according to the Gibb's principle of statistical thermodynamics by

$$f = f_0 \exp[\Delta E(\Delta H)/kT] \quad (6)$$

in which $\tau_0 = 1/f_0 \approx 10^{-9}$ s is the atomic reorganization time (time interval between two thermal excitations), $f_0 = f_0(T, m, H_K, H, \varphi)$ is a function of the temperature T , the particle magnetic moment m , the microcoercivity H_K , and the applied field H and its orientation φ with respect to the easy axis. The frequency f_0 results from the solution of physical equations which describe thermal activation processes in terms of Brownian motion of the particle moment [Brown, 1963]. For $\varphi = 0$ and $\mu_0 m H_K \gg kT$, Brown [1963] gives the following approximate solution when the initial magnetization is antiparallel to the applied field:

$$f_0 \approx \frac{\mu_0 \gamma_0}{2} H_K \sqrt{\frac{\alpha}{\pi}} (1+h)(1-h)^2 \left(1 + \frac{1+h}{1-h} e^{-4\alpha h} \right) \quad (7)$$

in which γ_0 is the gyromagnetic ratio, $\alpha = \mu_0 m H_K / 2kT$ the reduced energy barrier and $h = H/H_K$ the reduced field. *Aharoni* [1964] calculated f_0 numerically for $\varphi = 0$ and different values of α and h , showing that the relative error of equation (7) is within 30% when $\alpha > 5$ and $h < 0.5$. For $\alpha > 5$ and $h > 0.7$ the relative error of equation (7) can reach one order of magnitude. *Néel* [1949] gives a similar expression for f_0 , based on piezomagnetic induced activation.

[22] In our case, with $H = H_K - \Delta H$, we obtain from equation (7) for $\Delta H \ll H_K$ and $\alpha > 20$ (SD particles):

$$f_0 \approx \mu_0 \gamma_0 H_K \sqrt{\frac{\alpha}{\pi}} \left(\frac{\Delta H}{H_K} \right)^2 \quad (8)$$

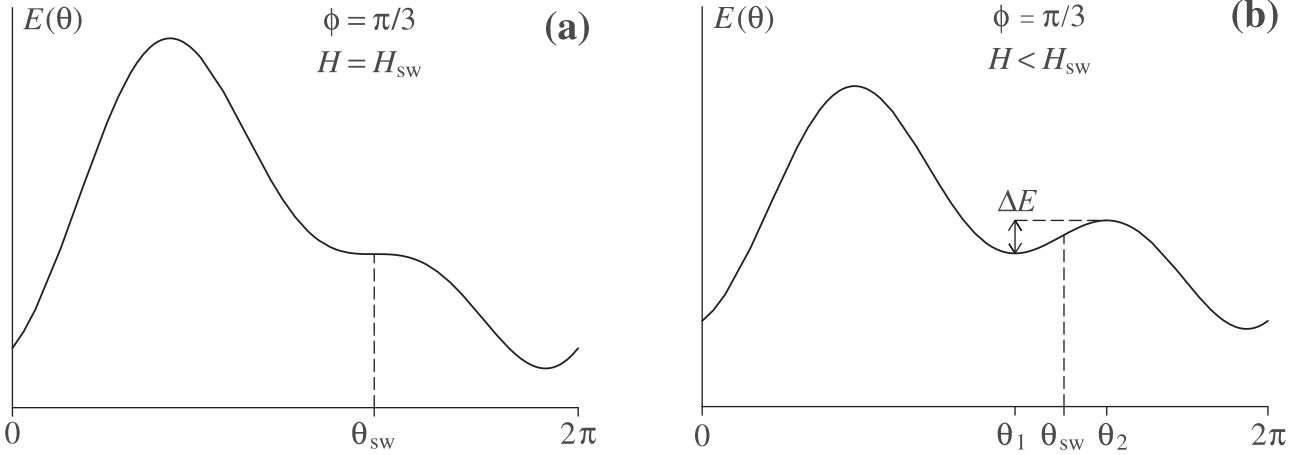


Figure 4. Free energy of a SD particle as a function of the angle θ of the magnetic moment with respect to the easy axis (a) when a field equal to the switching field is applied and (b) when a field slightly smaller than the switching field is applied. ΔE is the energy barrier to overcome for a switching event.

This approximation is not accurate for $\Delta H \rightarrow 0$ and is strictly valid only in the special case of $\varphi = 0$. Since an accurate and general solution for f_0 is not reported in the literature, we assume

$$f_0 = F_0(T, m, H_K) \Delta h^q \quad (9)$$

where $\Delta h = \Delta H/H_K$ and q is an exponent which depends on the model chosen to explain thermal activation. For $q = 0$ one has the intuitive model in which $F_0 = 1/\tau_0 = \text{const}$. Equation (8) is a particular case of equation (9) with $q = 2$ when the initial magnetization is antiparallel to the applied field. For the same configuration and $\Delta h \ll 1$, Néel [1949] gives $q = 3/2$. Brown [1959] demonstrated that different theories with q ranging from 1 to 2 lead substantially to the same results, because the dependence of the activation frequency on the exponential term of equation (6) dominates over the dependence of f_0 on the applied field. We will show later in this section that the calculated ARM is almost independent from the value chosen for q , so that a precise estimation of f_0 is not necessary.

[23] Now, in contrast to section 1, both orientations of the particle moment, parallel (upward arrow) and antiparallel (downward arrow) to h_{DC} , are possible, even if $|H| < H_{sw}$. This can be considered as a reduction of the effective switching field of the particle by a “fluctuation field”, according to Néel [1955]. We consider a large number N of identical particles with the same orientation of their easy axis and the same H_K . Let m_{\parallel} be the component of the magnetic moment parallel to the applied field. We assume that m_{\parallel} of a proportion p of these particles ($0 \leq p \leq 1$) is positive (upward arrow), and the remainder $(1 - p)$ is negative (downward arrow). Switching events occur with high probability at minima of the applied field for the positively magnetized part p and at maxima of the applied field for the other part, according to Figure 3b.

[24] The switching frequency f_{\pm} in the two cases is given according to equations (6) and (9) and $h_{DC} = H_{DC}/H_K$ by

$$f_{\pm} = F_0(\Delta h \pm h_{DC})^q \exp\left(-\frac{\Delta E(\Delta h \pm h_{DC})}{kT}\right) \quad (10)$$

3.3. Estimation of the Energy Barriers

[25] Let θ_{sw} be the value of θ at which a switching of the moment occurs in the Stoner-Wolfarth model. Except when $\varphi = 0$ and $\varphi = \pi/2$, θ_{sw} represents a horizontal flex point on the plot of $\varepsilon(\theta)$ (Figure 4a). Since the amount of particles whose easy axis define an angle φ with the applied field is proportional to $\sin \varphi$, and their contribution to the remanent magnetization parallel to the applied field is proportional to $\sin \varphi \cos \varphi$, the special cases $\varphi = 0$ and $\varphi = \pi/2$ do not contribute to the ARM and can be ignored. Victoria [1989] estimated the energy barrier ΔE to overcome for a moment switching when the applied field is slightly smaller than H_{sw} by setting $\partial E/\partial \theta = \partial^2 E/\partial \theta^2 = 0$ and $\varphi \neq 0, \pi/2$:

$$\Delta E = \varepsilon_{sw} \mu_0 m H_K \Delta h^{3/2} \quad (11)$$

with $\varepsilon_{sw} = (2/3)^{3/2} \sin 2\theta_{sw}/h_{sw}^{3/2}$. This expression is substantially different from the result obtained by Néel [1949] for aligned particles: $\Delta E = \mu_0 m H_K \Delta h^2/2$. In Figure 5 the approximate solution for ΔE given in equation (11) for a small energy barrier is compared to the numerical result obtained directly from equation (1). A very good agreement is found also with higher energy barriers.

3.4. Changes of the Particle Moment With Time in a Biased Alternating Field

[26] Equation (10) can now be rewritten as

$$f_{\pm} = F_0 \Delta h^q \left(1 \pm \frac{h_{DC}}{\Delta h}\right)^q \exp\left[-\alpha \Delta h^{3/2} \left(1 \pm \frac{h_{DC}}{\Delta h}\right)^{3/2}\right] \quad (12)$$

with $\alpha = \varepsilon_{sw} \mu_0 m H_K/kT$. The switching frequency f_{\pm} is modulated in time by the frequency of the AC field. This allows us to define the mean switching frequency \bar{f}_{\pm} . For simplicity, we consider first

$$f = F_0 \Delta h^q \exp(-\alpha \Delta h^{3/2}) \quad (13)$$

The switching frequency f_{\pm} can be obtained from equation (13) by substitution of Δh with $\Delta h \pm h_{DC}$. The modulation

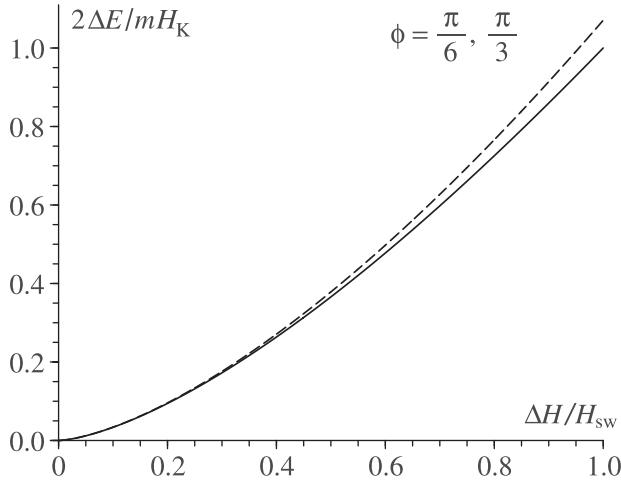


Figure 5. Energy barrier of a SD particle which has to be overcome for a switching event, when a field $H_{sw} - \Delta H$ is applied. The solid line represents the exact solution. The analytical approximation given in the text is represented by the dashed line, computed for the symmetrical points $\varphi = \pi/6$ and $\varphi = \pi/3$ in Figure 3b.

in time of $f = f(t)$ according to equation (13) is represented in Figure 6b over one period. The corresponding mean frequency \bar{f} is given by

$$\bar{f}(t) = 2f_{AC} \int_t^{t+1/2f_{AC}} f(\tau) d\tau \quad (14)$$

Equation (14) cannot be evaluated analytically, except for the limit cases of $\Delta\bar{h} \rightarrow 0$ and $\Delta\bar{h} \rightarrow h_{sw}$. Since $\Delta\bar{h}$ changes with time, the two limits are reached at the

beginning and at the end of the acquisition process, respectively. The magnetic moment of a particle blocks when $\Delta\bar{h}$ grows from 0 to h_{sw} . Superparamagnetic particles are thermally activated even without the help of an external field: they remain unblocked at the end of the acquisition process, when $\Delta\bar{h} = h_{sw}$, and their magnetization is unstable. In this case the mean switching frequency is given by (13) when Δh is replaced by $\Delta\bar{h}$:

$$\bar{f}(t) \approx F_0 \Delta\bar{h}^q \exp[-\alpha \Delta\bar{h}^{3/2}] \quad (15)$$

The moment of larger particles blocks earlier, when $\Delta\bar{h} < h_{sw}$. The limit case of $\Delta\bar{h} \ll h_{sw}$ is a good approximation for large, stable SD particles. In this case, since f decreases rapidly with increasing values of Δh , as shown in Figure 6a, $\Delta h(t)$ can be conveniently approximated by a parabola:

$$\Delta h(t) \approx \Delta\bar{h} + \frac{1}{2} (h_{sw} - \Delta\bar{h}) (2\pi f_{AC} t)^2 \quad (16)$$

and equation (13) becomes

$$f(t) = F_0 \Delta\bar{h}^q (1 + bt^2)^q \exp[-a(1 + bt^2)^{3/2}] \quad (17)$$

$$a = \alpha \Delta\bar{h}^{3/2} \quad b = \frac{h_{sw} - \Delta\bar{h}}{2\Delta\bar{h}} (2\pi f_{AC})^2$$

The magnetic moment of a particle blocks when $\Delta\bar{h}$ reaches a value $\Delta\bar{h}_0$ given later in this section by equation (25). In general, $a \gg 1$ when $\Delta\bar{h}$ is of the same order of magnitude as $\Delta\bar{h}_0$: $a \approx 14$ with $\mu_0 H_K = 60$ mT and $m = 5 \times 10^{-17}$ A m². For SD magnetite grains that switch by coherent rotation, $\mu_0 H_K < 300$ mT and $m < 10^{-16}$ A m² [Newell and Merrill, 1999], and consequently, using equation (25), $a > 8$. For reasons explained later, the

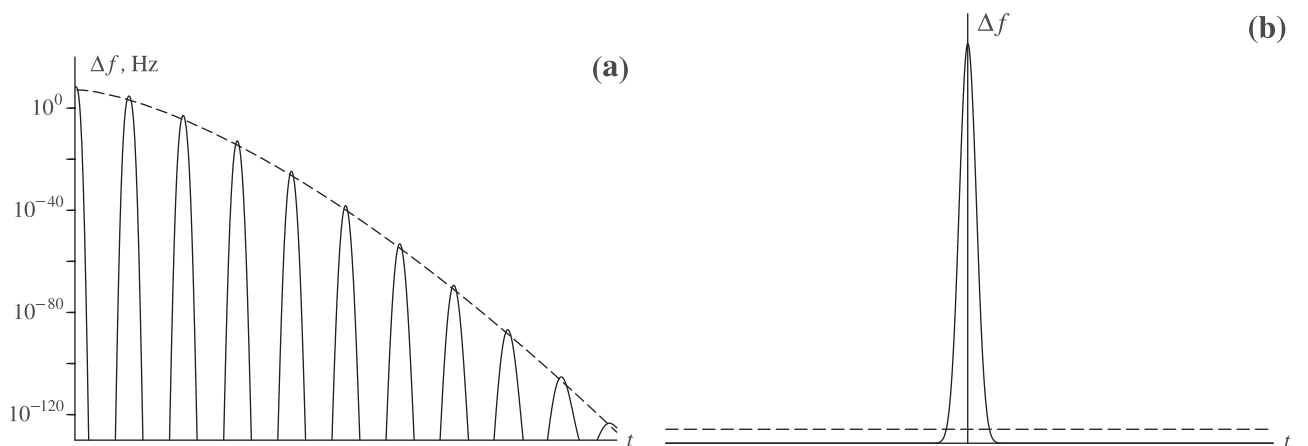


Figure 6. (a) The instantaneous net switching frequency (solid line) over a complete ARM cycle for a magnetite SD particle and the mean net switching frequency, averaged over one period of the AF field. The switching frequency was calculated with following data: $T = 300$ K, $m = 4 \times 10^{-17}$ A m², $\mu_0 H_K = 60$ mT, and $\mu_0 H_{DC} = 100$ μ T. The number of periods over the ARM cycle has been reduced for clarity: an ARM cycle contains typically several hundreds of periods. (b) Calculation of the mean switching frequency (dashed line) over one period. The area under the curve represents the number of switching events over one period, which is identical to that defined by the instantaneous switching frequency (solid line). The scale on the frequency axis is linear.

estimation of f_{\pm} is important only for values of $\Delta\bar{h}$ around $\Delta\bar{h}_0$, and $a \gg 1$ can be assumed in equation (17). Then equation (14) has the approximate analytical solution:

$$\bar{f}(t) \approx F\Delta\bar{h}^{q-1/4} \exp\left[-\alpha\Delta\bar{h}^{3/2}\right] \quad (18)$$

valid for the limit case of $\Delta\bar{h} \ll h_{sw}$, whereby $F = F_0(3\pi h_{sw}\alpha)^{-1/2}$. Equations (15) and (18) differ only in the preexponential factor, which has little influence on the final result. Since the measured ARM magnetization is carried mainly by stable particles, equation (18) is adopted as a general solution of (14). From equations (12) and (18) we have then the mean switching frequency:

$$\bar{f}_{\pm}(t) = F(\Delta\bar{h} \pm h_{DC})^{q-1/4} \exp\left[-\alpha(\Delta\bar{h} \pm h_{DC})^{3/2}\right] \quad (19)$$

We assume $h_{DC} \ll \Delta\bar{h}$ for the DC fields normally used in ARM experiments, and in the critical time interval during which the magnetic moment blocks, that is, when $\Delta\bar{h} \approx \Delta\bar{h}_0$. For example, $\mu_0 H_k \Delta\bar{h} > 1$ mT for particles with $\mu_0 H_K > 2$ mT and $m < 10^{-16}$ A m² (practically all SD magnetites that switch by coherent rotation). When $\Delta\bar{h} \approx \Delta\bar{h}_0$, then $\Delta\bar{h} \gg \alpha^{-2/3}$ and equation (19) simplifies to

$$\bar{f}_{\pm}(t) = F\Delta\bar{h}^{q-1/4} \exp\left[-\alpha\Delta\bar{h}^{3/2}\right] \exp\left[\mp\frac{3}{2}\alpha\Delta\bar{h}^{1/2}h_{DC}\right] \quad (20)$$

Defining $M_s = Nm$ as the saturation magnetization, the net magnetization M_{\parallel} parallel to the applied field is given by $M_{\parallel} = (2p - 1)M_s \cos \varphi$ and the net change in time by

$$\frac{dM_{\parallel}}{dt} = 2M_s[(1-p)f_- - pf_+] \cos \varphi \quad (21)$$

Normalizing the magnetization with $\mu = M_{\parallel}/M_s \cos \varphi$ and substituting equation (20) in equation (21) gives the following differential equation in $\mu(\Delta\bar{h})$:

$$\frac{d\mu}{d\Delta\bar{h}} = -a(\mu - \mu_{\infty}) \quad (22)$$

$$a = \frac{F}{f_{AC}\Delta\bar{h}} \Delta\bar{h}^{q-1/4} \frac{\cosh\left[3\Delta\bar{h}^{1/2}\alpha h_{DC}/2\right]}{\exp\left[3\Delta\bar{h}^{3/2}\alpha/2\right]}$$

$$\mu_{\infty} = \tanh\left[\frac{3}{2}\alpha\Delta\bar{h}^{1/2}h_{DC}\right]$$

which does not have an analytical solution. The coefficients of equation (22) depend on time through $\Delta\bar{h}(t) = 2f_{AC}\Delta\bar{H}t$. To find an approximate solution of equation (22), we solve first the stationary case, in which $\Delta\bar{h}$ is constant. Thus, we put $\Delta\bar{h} = \Delta\bar{h}_0$ on the right side of equation (22) and obtain with the initial condition $\mu = 0$ at $t = 0$ the solution:

$$\mu(\Delta\bar{h}, \Delta\bar{h}_0) = \mu_{\infty} [1 - \exp(-a(\Delta\bar{h}_0)\Delta\bar{h})] \quad (23)$$

[27] Thermodynamic equilibrium is given by the value $\mu_{\infty}(\Delta\bar{h}_0)$ of μ as $t \rightarrow \infty$, and is reached after a character-

istic time which corresponds to $\Delta\bar{h}_{eq} = 1/a$. If the time-dependent coefficient a in equation (22) does not change significantly over the characteristic time which corresponds to $\Delta\bar{h}_{eq}$, that is, when $\Delta\bar{h}_0 \gg \Delta\bar{h}_{eq}$, the asymptotic solution $\mu = \mu_{\infty}(\Delta\bar{h}_0)$ in equation (23) is a good approximation of the general solution, and the magnetization is in thermodynamical equilibrium with the applied field. As time proceeds, $\Delta\bar{h}_0$ increases and the coefficient becomes progressively smaller. As a consequence, also the change in magnetization with time becomes smaller, until a final value of μ is reached. Because of the exponential dependence of a on time, the blocking process is sharp, and we can assume the final magnetization to represent the thermodynamic equilibrium μ_{∞} reached just before it becomes frozen in. We assume that this occurs when $\Delta\bar{h}_0 = \gamma\Delta\bar{h}_{eq}$, where γ is an unknown constant in the order of 1. This leads to the following transcendental equation in $\Delta\bar{h}_0$:

$$\Delta\bar{h}_0 = \frac{\gamma f_{AC}\Delta\bar{h}}{F} \Delta\bar{h}_0^{1/4-q} \frac{\exp\left[\alpha\Delta\bar{h}_0^{3/2}\right]}{\cosh\left[3\alpha\Delta\bar{h}_0^{1/2}h_{DC}/2\right]} \quad (24)$$

With $\alpha \gg 1$ and assuming $q = 3/4$, for reasons explained later, equation (24) has the approximate solution:

$$\Delta\bar{h}_0 \approx \alpha^{-2/3} \ln^{2/3} \left[\frac{5.7F_0}{\gamma f_{AC}\Delta\bar{h} h_{sw}^{1/2} \alpha^{3/2}} \right] \quad (25)$$

Inserting this result in equation (23) gives the final magnetization μ_{∞} as $t \rightarrow \infty$:

$$\mu_{\infty} \approx \tanh \left[\frac{3}{2}\alpha^{2/3} \ln^{1/3} \left(\frac{5.7F_0}{\gamma f_{AC}\Delta\bar{h} h_{sw}^{1/2} \alpha^{3/2}} \right) h_{DC} \right] \quad (26)$$

To estimate a numerical value of γ , we linearize equation (23) for $h_{DC} \rightarrow 0$ and obtain

$$\frac{d\mu}{d\Delta\bar{h}} = -\frac{F}{f_{AC}\Delta\bar{h}} \Delta\bar{h}^{q-1/4} \exp\left[-\frac{3}{2}\alpha\Delta\bar{h}^{3/2}\right] \left(\mu - \frac{3}{2}\alpha\Delta\bar{h}^{1/2}h_{DC} \right) \quad (27)$$

Equation (27) can be scaled as follows:

$$y' = -\kappa\tau^{2q+1/2} \left(y - \frac{3}{2}\tau \right) \exp(-\tau^3) \quad (28)$$

$$\kappa = \frac{2F_0}{\sqrt{3\pi}h_{sw}f_{AC}\Delta\bar{h}\alpha^{1+2q/3}}$$

where $\tau = \alpha^{1/3}\sqrt{\Delta\bar{h}}$ is the scaled time, $y = \alpha^{-2/3}h_{DC}^{-1}\mu$ is the scaled magnetization and κ a parameter of the equation. Equation (28) is not analytically solvable and has nonconstant coefficients. Numerical solutions of equation (28) for different values of κ , ranging from 100 to 10^{14} , and for $q = 0, 1, 3/2, 2$ were computed with the software Mathematica, starting from the initial condition $y(\tau = 0) = 0$, until saturation was reached, at $\tau \approx 5$. Results for $q = 0$ are plotted in Figure 7a. For high values of κ the sharp transition from thermodynamic equilibrium to a ‘‘frozen’’

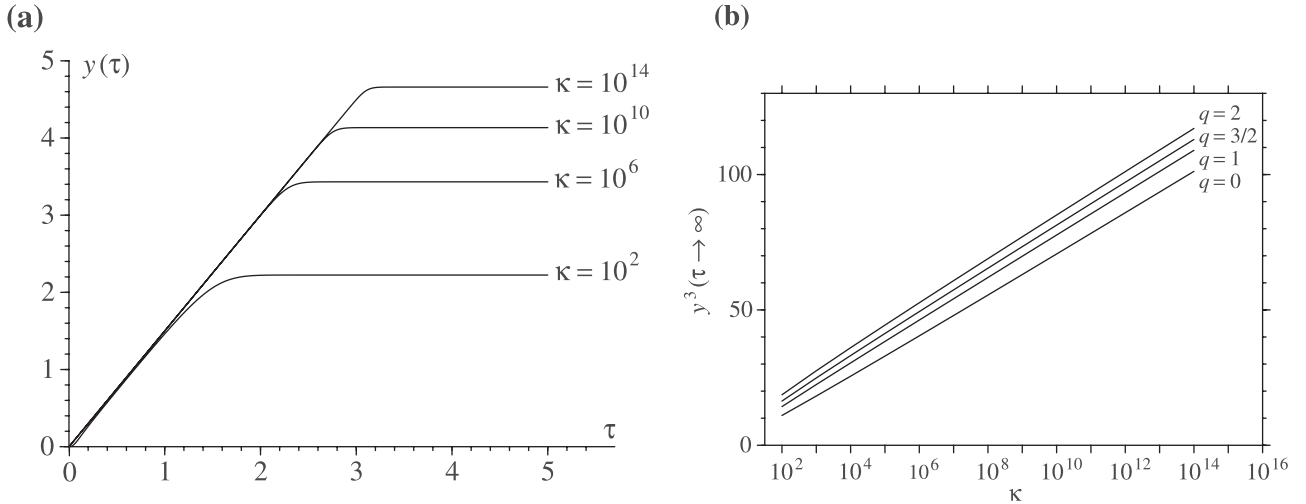


Figure 7. (a) Solutions of the differential equation (29) for different values of the parameter κ . The parameter τ is an expression for the time during an ARM cycle, and $y(\tau)$ an expression of the magnetization acquired by a SD particle. The flat part of the curves represents the final magnetization acquired, and is a function of κ . (b) The final value of the magnetization as a function of the parameter κ for different switching models expressed by the parameter q . The solutions show only a weak dependence on the switching model.

situation is evident. The asymptotic value for $\tau \rightarrow \infty$ from the numerical solutions, which represents the final ARM acquisition, is plotted in Figure 7b. The $\ln^{1/3}$ term in equation (26) is confirmed by the numerical solutions. A linear interpolation of the solutions of Figure 7b gives

$$y^3(\tau \rightarrow \infty) \cong c_1 + c_2 \ln \kappa \quad c_1 = -4.918 + 4.196q, \\ c_2 = 3.275 + 0.135q \quad (29)$$

for $0 \leq q \leq 2$. Table 1 gives the numerical solutions of $y(\tau \rightarrow \infty)$ for typical SD magnetite with $m = 4 \times 10^{-17}$ A m², $\mu_0 H_K = 60$ mT, $T = 300$ K, $f_{AC} = 400$ Hz, and $\mu_0 \Delta \tilde{H} = 5$ μ T and different thermal activation models. Models with different values of q , representing significantly different activation models, result in very similar solutions for $y(\tau \rightarrow \infty)$ ranging from 3.1 to 3.9.

3.5. Solution for ARM From the Kinetic Equation

[28] Next we adopt the solution given by $q = 3/4$ because of its algebraic simplicity. For $h_{DC} \rightarrow 0$ we then obtain from equation (29) the approximate solution:

$$\mu_\infty = \frac{3}{2} \alpha^{2/3} \ln^{1/3} \left[\frac{1.18 F_0}{f_{AC} \Delta \tilde{h} h_{sw}^{1/2} \alpha^{3/2}} \right] h_{DC} \quad (30)$$

The solutions given in equations (26) and (30) are almost identical for $h_{DC} \rightarrow 0$. We recall that these solutions are valid for a given direction φ of the easy axis with respect

to the applied field. For an isotropic assembly of particles the distribution density of their easy axis is given by $\sin \varphi$. The contribution of all orientations to the bulk magnetization parallel to the applied field is then given by

$$M = 0.5 M_s \int_0^{\pi/2} \mu_\infty(\varphi) \sin 2\varphi d\varphi \quad (31)$$

which finally gives together with equation (30): $M = \chi_{ARM} H_{DC}$, with a finite susceptibility of ARM:

$$\chi_{ARM} = 1.797 \mu_0 M_{rs} \left(\frac{m}{kT \sqrt{\mu_0 H_K}} \right)^{2/3} \ln^{1/3} \left[\frac{0.35 F_0}{f_{AC} \Delta \tilde{h} \sqrt{\mu_0 H_K}} \left(\frac{kT}{m} \right)^{3/2} \right] \quad (32)$$

and $M_{rs} = 0.5 M_s$. Equation (32) is formally equivalent to a special case of equation (30) with $h_{sw} = 0.528$, which corresponds to $\varphi = 61^\circ$. It is also very similar to equation (4) with $\varphi = \pi/4$. According to the result of section 1, where thermodynamic activation was ignored, $\chi_{ARM} \rightarrow \infty$ for $T \rightarrow 0$.

[29] Considering equation (30) as a limit case of equation (26), we obtain the final expression for the ARM acquisition curve:

$$M(H_{DC}) = M_{rs} \tanh(\chi_{ARM} H_{DC} / M_{rs}) \quad (33)$$

Table 1. Comparison of the Numerical Solutions of Different Activation Models

| Activation Model | q | F_0 , GHz | Estimation Source | $y(\tau \rightarrow \infty)$ |
|-------------------|-----|-------------|----------------------------|------------------------------|
| Intuitive model | 0 | 1–10 | Butler and Banerjee [1975] | 3.7–3.9 |
| Gyrom. precession | 1 | 1–10 | Brown [1959] | 3.3–3.5 |
| Magnetostriction | 1.5 | 10,000 | Néel [1955] | 3.9 |
| Brownian motion | 2 | 20–200 | Brown [1959] | 3.1–3.4 |

Equation (32) is extremely weakly dependent on the parameters of the AC field: a change of a factor 10 in frequency or decay rate produces a change of only 4% in χ_{ARM} of typical SD magnetite.

[30] The results of this section were obtained assuming uniform rotation of the magnetization during the switching of the particle moment. However, several studies [e.g., *Aharoni and Shtrikman*, 1958] have shown that the magnetization of large SD grains during a moment switching is nonuniform, and exhibits a so-called curling or vortex configuration. This configuration lowers the energy barrier necessary to switch the moment and consequently the coercivity of the particle. Results of micromagnetic calculations of the energy barrier in magnetite cubes by *Enkin and Williams* [1994] are reproduced in Figure 12 in section 5 and show a drop of the energy barrier for sizes larger than 60 nm. As result, the energy barrier calculated in equation (11) may be considered as an upper limit, especially for grain sizes near the SD/PSD boundary. Other expressions for the field dependence of the energy barrier do not affect the form of the differential equation (22), which leads to the same kind of solution as in equation (32). A lower energy barrier increases the relative importance of the thermal energy and is therefore equivalent to an apparent increase of temperature. This produces a decrease of the susceptibility of ARM, so that equations (32) and (33) have to be considered as an upper limit for the ARM acquisition of SD particles.

[31] Equation (32) predicts an increase of the susceptibility of ARM with grain size in the SD range. For SD magnetite, according to the coherent rotation model, H_K is independent of the grain size, and thus, the susceptibility of ARM is proportional to d^2 , where d is the diameter of the particles. The dependence of ARM on the grain size for particles smaller than 60 nm will be verified experimentally in sections 5 and 6.

4. Fluctuation Field

4.1. Previous Studies

[32] The field which is necessary to reverse the magnetic moment of a SD particle by overcoming the energy barrier due to anisotropy was called switching field H_{sw} in section 2. Thermal activation is responsible for the moment switching even when the applied field is smaller than H_{sw} . It has the effect of reducing H_{sw} by an amount H_q , which *Néel* [1949] called a “fluctuation field”. The fluctuation field depends on the moment of the particle and the time needed to switch its direction. In the literature a distinction is made between H_{sw} , often called the “microscopic coercive force H_c ”, and the field at which a moment-reversal occurs under specified conditions of time and temperature. The latter is called the “unblocking field H_B ” and is the difference between H_c and H_q ; that is, $H_B = H_c = H_q$ [*Dunlop and West*, 1969]. Simple calculations based on the application of thermal activation theory to a set of oriented particles give the following commonly quoted expression for H_q [*Dunlop and West*, 1969]:

$$H_q = H_K \sqrt{\frac{2kTH_q}{\mu_0 m H_K} \ln\left(\frac{F_0 \tau}{2} \frac{H_q^2}{H_K^2}\right)} \quad (34)$$

where τ is the time necessary to switch the magnetic moment. In case of AF demagnetization, $\tau \approx 1/f_{\text{AC}}$ [*Kneller and Wolfarth*, 1966].

4.2. Fluctuation Field of Identical, Aligned Particles

[33] In this paragraph we define the fluctuation field on the base of AF demagnetization curves as the difference between the real median destructive field and the theoretical value obtained by ignoring thermal activation effects. AF demagnetization can be conveniently described in a similar way as in section 3 by considering it to be a special case of ARM with $H_{\text{DC}} = 0$. An expression is obtained for the fluctuation field of randomly oriented particles, which shows important differences in comparison to equation (34).

[34] Again we consider the behavior of noninteracting SD particles in the magnetic field of Figure 1, but now $H_{\text{DC}} = 0$. The particles are identical and have a given orientation φ of their easy axes with respect to the applied field. If thermodynamic effects are neglected, the initial magnetization M_0 remains unaffected if the initial amplitude \tilde{H}_0 of the alternating field is less than the switching field $H_{\text{sw}} = h_{\text{sw}}(\varphi)H_K$. For $\tilde{H}_0 \geq H_{\text{sw}}$, the sample is fully demagnetized, leading to a final magnetization $M = 0$.

[35] Thermal activation is responsible for the switching of the particle moments even when $\tilde{H}_0 < H_{\text{sw}}$. The problem of thermal activation in a decaying AC field was analyzed in section 3, leading to the differential equation (22). The special case $h_{\text{DC}} = 0$ of equation (22):

$$\frac{d\mu}{d\Delta\bar{h}} = \frac{-F}{f_{\text{AC}}\Delta\bar{h}} (\Delta\bar{h})^{q-1/4} \exp\left[-\alpha\Delta\bar{h}^{3/2}\right] \mu \quad (35)$$

describes the time evolution of the normalized magnetization μ during the demagnetization. We assume an initial magnetization $\mu = 1$, when $\Delta\bar{h}(t=0) = \Delta\bar{h}_0$. Integration of equation (35) gives

$$\ln \mu(\Delta\bar{h}) = \frac{-F}{f_{\text{AC}}\Delta\bar{h}} \int_{\Delta\bar{h}_0}^{\Delta\bar{h}} u^{q-1/4} \exp\left(-\alpha u^{3/2}\right) du \quad (36)$$

Equation (36) has an analytical solution in the special case of $q=3/4$. Since equation (22) is almost independent of q , as demonstrated in section 3, we choose $q = 3/4$ as an excellent approximation for the general case and obtain

$$\mu(\Delta\bar{h}_0, \Delta\bar{h}) = \exp\left[\frac{2F}{3f_{\text{AC}}\Delta\bar{h}\alpha} \left(\exp\left(-\alpha\Delta\bar{h}^{3/2}\right) - \exp\left(-\alpha\Delta\bar{h}_0^{3/2}\right)\right)\right] \quad (37)$$

The end of the demagnetization process can be identified with $\Delta\bar{h} \rightarrow \infty$, leading to the final magnetization expressed by

$$\mu_{\infty}(\Delta\bar{h}_0) = \exp\left[-\frac{2F}{3f_{\text{AC}}\Delta\bar{h}_0\alpha} \exp\left(-\alpha\Delta\bar{h}_0^{3/2}\right)\right] \quad (38)$$

The final magnetization μ_{∞} as a function of the initial value $\Delta\bar{h}_0$ of $\Delta\bar{h}$ is plotted in Figure 8 for different values of H_K and m and is characterized by a sharp transition

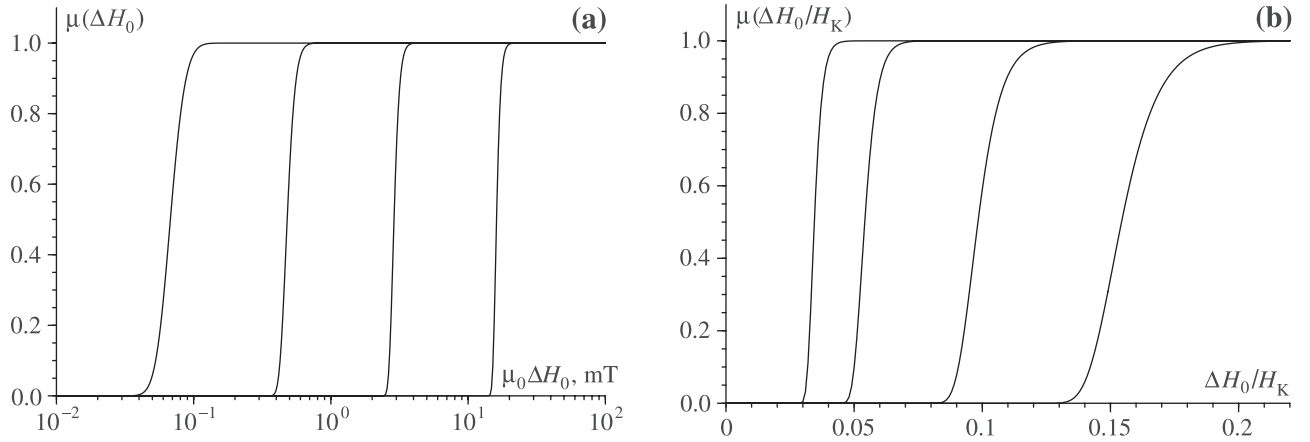


Figure 8. Normalized magnetization of an oriented assemblage of noninteracting SD particles with microcoercivity H_K , after AF demagnetization with an initial peak field equal to $H_{sw} - \Delta H_0$, H_{sw} being the switching field. (a) The dependence of H_q on the particle moment and (b) the dependence on the microcoercivity. The value of ΔH_0 , at which $\mu = 0.5$, is defined as the fluctuating field H_q of the particles. For large moments the fluctuation field is very small and the particles behave according to the Stoner-Wolfarth theory. The magnetization is calculated with equation (38) with following parameters: $T = 300$ K, $f_{AC} = 400$ Hz, $\mu_0 \Delta \tilde{H} = 5$ μ T, $\varphi = \pi/3$, and (a) $\mu_0 H_K = 60$ mT with $m \times 10^{-18}$, 5×10^{-17} , 5×10^{-16} , 5×10^{-15} A m² from left to right, (b) $m = 5 \times 10^{-17}$ A m² with $\mu_0 H_K = 100, 50, 20, 10$ mT from left to right.

from $\mu_\infty \rightarrow 0$ for small values of $\Delta \tilde{h}_0$ to $\mu_\infty \rightarrow 1$ for large values of $\Delta \tilde{h}_0$. We define the fluctuation field H_q as the value of $\Delta \tilde{h}_0$ for which the magnetization is reduced to half its initial value. Since the transition is sharp, the choice of the fraction of initial magnetization is not relevant. From equation (38) we then obtain the equation $\mu_\infty(H_q) = 0.5$, with solution

$$H_q = \left(\frac{kT}{\mu_0 f_{sw} m} \right)^{2/3} \ln^{2/3} \left[\frac{2F_0}{3 \ln 2 \sqrt{3} \pi \mu_0 h_{sw} H_K f_{AC} \Delta \tilde{H}} \left(\frac{kT}{f_{sw} m} \right)^{3/2} \right] \quad (39)$$

4.3. Fluctuation Field of Identical, Randomly Oriented Particles

[36] We generalize now to the case of a sample with identical randomly oriented particles. Let $\mu(\varphi) \cos \varphi \sin \varphi$ be the contribution of all particles with orientation φ to the total magnetization. In case of an IRM, $\mu(\varphi) = 1$. In case of an ARM, $\mu(\varphi)$ is given by equation (30) when $h_{DC} \rightarrow 0$. The total magnetization $\mu_\infty^{\text{tot}}(\Delta \tilde{h}_0)$ after the AF demagnetization is given by

$$\mu_\infty^{\text{tot}}(\Delta \tilde{h}_0) = \int_0^{\pi/2} \mu(\varphi) \exp \left[-\kappa \exp \left(-\alpha \Delta \tilde{h}_0^{3/2} \right) \right] \sin 2\varphi \, d\varphi \quad (40)$$

Equation (40) cannot be evaluated analytically. Numerical solutions for SD grains with different moments and $H_K = 60$ mT, $f_{AC} = 400$ Hz, $\Delta \tilde{H} = 5$ μ T are represented in Figure 9 as a function of the maximum AC peak field \tilde{H} .

[37] Defining again H_q as the solution of the equation $\mu_\infty^{\text{tot}}(H_q) = 0.5$, one has the numerical results of Table 2, given for different values of the particle moment with $H_K = 60$ mT and the same parameters as Figure 9. The

value of φ in equation (39) which gives the calculated H_q in (40) is also given in Table 2: it has a mean of $\varphi = 62^\circ$ and differs by no more than 1° when the particle moment varies by over 3 orders of magnitude. We assume therefore equation (39) with $\varphi = 62^\circ$ as an excellent approximation of the

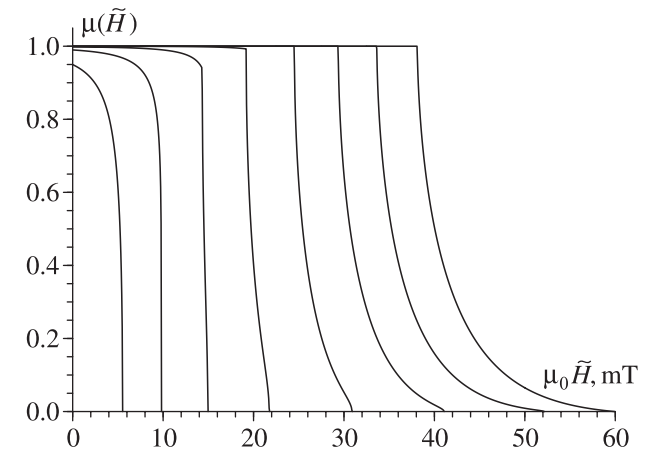


Figure 9. Normalized AF demagnetization curves of randomly oriented, non-interacting magnetite SD particles with $\mu_0 H_K = 60$ mT and different magnetic moments, from left to right: 2.0×10^{-18} , 2.4×10^{-18} , 3.0×10^{-18} , 4.0×10^{-18} , 6.0×10^{-18} , 1.0×10^{-17} , 2.0×10^{-17} , 1.0×10^{-16} A m². The last curve on the right is the AF demagnetization without thermal activation, according to the classic Stoner-Wolfarth model. Other parameters are $T = 300$ K, $f_{AC} = 400$ Hz, and $\mu_0 \Delta = 5$ μ T. The difference between the median destructive field of the curves with and without thermal activation can be identified with the fluctuation field of the particles. According to the Néel relaxation theory a moment of 2.4×10^{-18} A m² has a relaxation time of 10 s.

Table 2. Numerical Calculation of the Fluctuating Field for Different Particle Moments

| Magnetic Moment, A m ² | Demagnetization of IRM | | Demagnetization of ARM | | Equation (34) H_q , mT |
|--------------------------------------|------------------------|----------------------------|------------------------|----------------------------|-----------------------------|
| | H_q , mT | φ in Equation (39) | H_q , mT | φ in Equation (39) | |
| 2.4×10^{-18} | 32.3 | 60.5 | 32.2 | 60.1 | 75.4 |
| 4.0×10^{-18} | 22.3 | 60.9 | 22.3 | 66.8 | 57.6 |
| 6.0×10^{-18} | 16.6 | 61.0 | 16.7 | 61.4 | 46.6 |
| 1.0×10^{-17} | 11.4 | 60.5 | 11.5 | 61.6 | 35.6 |
| 2.0×10^{-17} | 6.78 | 59.9 | 6.75 | 62.5 | 24.6 |
| 5.0×10^{-17} | 3.39 | 58.8 | 3.60 | 64.5 | 15.2 |
| 1.0×10^{-16} | 2.00 | 58.3 | 2.21 | 67.1 | 10.5 |

fluctuation field of an assembly of random oriented SD particles and get finally

$$H_q = 0.801 \left(\frac{kT\sqrt{H_K}}{\mu_0 m} \right)^{2/3} \ln^{2/3} \left[\frac{F_0}{3.8f_{AC}\Delta\tilde{H}\sqrt{\mu_0 H_K}} \left(\frac{kT}{m} \right)^{3/2} \right] \quad (41)$$

Equations (34) and (41) have the same qualitative dependence on T , H_K , and m but give quite different results. We choose as example SD particles with $H_K = 60$ mT and following parameters: $T = 300$ K, $\Delta\tilde{H} = 5$ μ T, $f_{AC} = 400$ Hz. Results for H_q from equations (34) and (41) as a function of the particles moment are shown in Figure 10. Equation (34) gives systematically higher values for H_q , especially near the SD/PSD limit, where the difference in H_q can reach up to one order of magnitude. There are two reasons for this difference. First, equation (41) is the direct solution of the kinetic equations of a SD particle in an alternating field. Second, equation (34) is strictly valid only in the very special case of particles with their easy axes oriented parallel to the field, whereby these particles do not contribute significantly to the total magnetization of an isotropic sample.

[38] For classic Stoner-Wolfarth particles, the median destructive field of a demagnetization curve is given by $H_{1/2} = 0.524H_K$. If the mean switching field H_{sw} of a set of identical particles is identified with $H_{1/2}$, in case of thermal fluctuations one has $H_{sw} = 0.524H_K - H_q$. The shape of a demagnetization curve for a set particles with different microcoercivities is then given by the distribution of the values of H_{sw} .

5. Range of An hysteretic SD Behavior of Fine Particles

[39] The stability range of SD particles of magnetite and other minerals has been investigated in several theoretical and experimental studies [Dunlop and West, 1969; Butler and Banerjee, 1975; Diaz Ricci and Kirschvink, 1992; Newell and Merrill, 1999]. Often, single critical sizes are assumed to define the size range of SD particles. In reality, the critical sizes depend on the magnetic property under consideration. For example, grains can have a SD saturation remanent state and then develop domain walls in reverse fields [Halgedahl and Fuller, 1980].

[40] In the following, we consider the stability range of SD particles with shape-controlled anisotropy from the point of view of an hysteretic processes, i.e., ARM and AF demagnetization. We equate the stability range with the validity range of the equations derived in section 3 for the ARM. As already pointed out, the calculations of this paper assume a uniform rotation as reversal mechanism for the

particle moment. Newell and Merrill [1999] used nucleation theory to calculate the upper limit volume of ellipsoidal magnetite particles which reverse by uniform rotation in a magnetic field parallel to their easy axis. As discussed in section 3, only a negligible part of all particles in an isotropic sample satisfy this condition. However, the application of nucleation theory in the general case is complex and still unsolved. We assume therefore the results of Newell and Merrill [1999] as an initial approximation. Their upper limit for uniform rotation is almost independent of the shape of the ellipsoid and varies between 50 and 70 nm in size. For larger volumes, the particles can still exhibit a SD remanence, but they reverse in the curling mode and this leads to smaller values of the susceptibility of ARM. For comparison, Butler and Banerjee [1975] give grain sizes between 100 nm and 1 μ m as the upper limit of SD magnetite prisms.

[41] On the other hand, a reduction of the volume increases the fluctuation field, and lowers therefore all coercivity parameters (H_c , H_{cr} , and $\tilde{H}_{1/2}$). In the extreme case when a coercivity parameter is reduced to zero, the particle can be considered to be effectively superparamagnetic (SP). To define the SP/SD boundary we choose the volume at which $\tilde{H}_{1/2} = 0$. The results, plotted in Figure 11a, are slightly smaller in comparison to those of Butler and Banerjee [1975] for a time constant of 100 s.

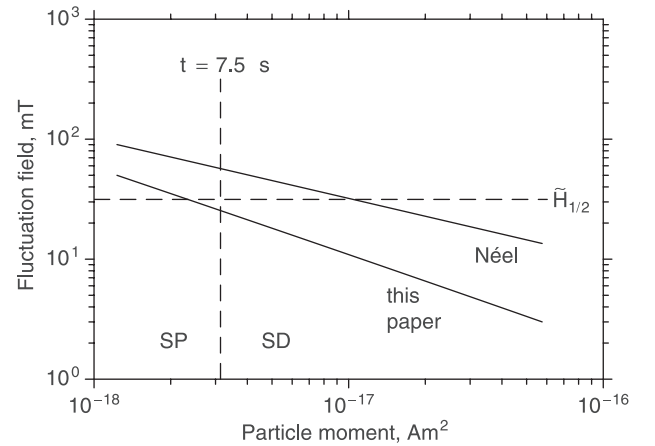
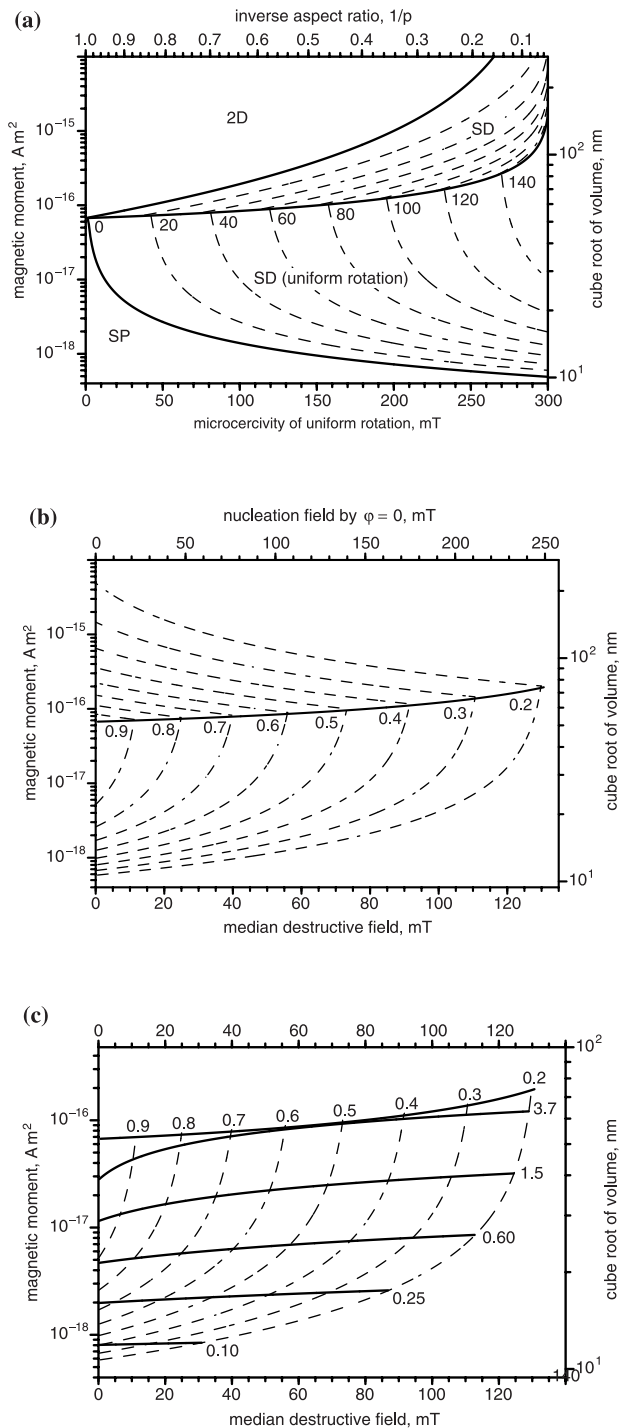


Figure 10. Comparison between the fluctuation field predicted by Néel theory and by the present theory for randomly oriented SD particles with $\mu_0 H_K = 60$ mT, as a function of the particle moment. The horizontal dashed line represents $\tilde{H}_{1/2}$ according to the Stoner-Wolfarth model, the vertical dashed line represents particles with a time constant $\tau = 7.5$ s, which is the time required by the AF field to decrease from $\tilde{H}_{1/2}$ to zero. A fluctuation field larger than $\tilde{H}_{1/2}$ represents an impossible solution.



[42] Stability ranges are commonly plotted as a function of the inverse shape parameter $1/p$, where p is the ratio of the largest to the shortest axis of a grain. For better characterization of the properties of SD magnetite, the stability range is plotted in Figure 11b as a function of the median destructive field or nucleation field. This method of plotting demonstrates more clearly than Figure 11a the transitional nature of the SP/SD and SD/PSD boundaries.

[43] The range of stability of SD particles increases with the shape parameter p , from $p = 0$ (a sphere) to $p = \infty$ (an infinite cylinder). Grains with large values of p are less likely to be observed in nature: often $0 \leq p \leq 2$. Magnetosomes have $p \approx 1$ (equant), $p \approx 1.5-2$ (prismatic), or $p \approx 3$ (bullet-shaped); fine-grained magnetite in soils has $p < 1.5$. Acicular magnetite can reach $p \approx 5$, as in the sample described in section 6. The parameter $\chi_{\text{ARM}}/\text{SIRM}$ can be calculated with equation (32) as a function of the magnetic moment m and the microcoercivity H_K , or the corresponding median destructive field. In Figure 11c, lines with constant $\chi_{\text{ARM}}/\text{SIRM}$ are plotted together with the stability diagram of Figure 11b. For common SD magnetite ($0 \leq q \leq 2$) and no interactions, $\chi_{\text{ARM}}/\text{SIRM}$ ranges from 2×10^{-4} m/A (for $m = 1.3 \times 10^{-18}$ A m^2 and $\mu_0 \tilde{H}_{1/2} = 20$ mT) to 3.7×10^{-3} m/A (for $m = 1 \times 10^{-16}$ A m^2 and $\mu_0 \tilde{H}_{1/2} = 70$ mT). Values between 2×10^{-4} m/A and 2.5×10^{-3} m/A are commonly measured in natural inorganic magnetite [Moskowitz *et al.*, 1993; Maher, 1988] and values up to 3.8×10^{-3} m/A have been reported in samples of intact magnetosomes [Moskowitz *et al.*, 1993]. Magnetic interaction between grains generally lowers the values of $\chi_{\text{ARM}}/\text{SIRM}$. This occurs with increasing concentration of the magnetic particles and has been observed experimentally [Banerjee and Mellema, 1974; Sugiura, 1979; Maher, 1988; Dunlop, 1981; Yamazaki

Figure 11. (opposite) Theoretical stability range for prolate ellipsoids of magnetite with shape anisotropy only. (a) Solid lines represent in order from bottom to top: upper limit for SP particles ($H_q = \tilde{H}_{1/2}$ in this paper); upper limit for a moment reversal by uniform rotation; upper limit for stable SD remanence (both after Newell and Merrill [1999]). Dashed lines represent the median destructive field for randomly oriented particles in the lower part of the stability diagram ($H_{1/2} = H_{\text{sw}} - H_q$ in this paper), and the nucleation field H_{curl} for curling in aligned particles in the upper part [after Newell and Merrill, 1999]. Numbers in the plot refer to $H_{1/2}$ and to $0.524H_{\text{curl}}$, respectively. (b) The solid line represents the upper limit for a moment switching by uniform rotation. Dashed lines represent lines of constant particle elongation p ; numbers refer to $1/p$. The lower part of the stability field represents the smallest volume of randomly oriented SD particles with elongation p as a function of their median destructive field. The upper part of the stability range represents the maximum volume of aligned particles with SD remanence as a function of the nucleation field for a moment switching by curling. (c) Same plot as Figure 11b for the region of moment switching by coherent rotation. Solid curves represent particles with same values of $\chi_{\text{ARM}}/\text{SIRM}$, expressed in 10^{-3} m/A by the numbers on the right. These values range from 10^{-4} to 2×10^{-3} m/A for common SD particles; the same values are measured in natural samples with SD grains.

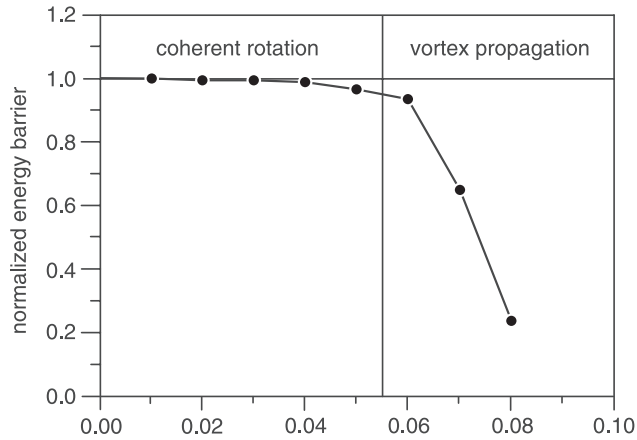


Figure 12. Energy barrier to magnetic moment reversal as a function of grain size in magnetite cubes. Incoherent rotation lowers the energy barrier over 60 nm grain size [from *Enkin and Williams, 1994*].

and Ioka, 1997]. The effect of interactions cannot be neglected in synthetic samples, where clustering of the magnetite particles is very difficult to avoid. Therefore ARM experiments on synthetic samples may not be representative for the situation encountered in natural samples with a low concentration of well-distributed magnetic grains.

[44] As already mentioned, the range of validity of equations (32) and (33) is limited to grain sizes related to a moment switching by coherent rotation. As demonstrated with micromagnetic calculations, the energy barrier of the moment switching drops significantly for grain sizes >60 nm (Figure 12). A significant change in the microcoercivity is

also expected. If the grains still exhibit SD remanence when the AF field is removed, new estimates of both microcoercivity and energy barrier allow extension of the thermal activation model toward larger grain sizes. Above the upper limit for SD remanence, magnetic grains can exhibit different remanence states which are influenced by the past history of the grain. The field applied during an ARM may induce the remanence state which minimizes the magnetic energy of the grain in the DC field, and this state is not influenced by thermal activation effects. The acquisition process of such grains is therefore fundamentally different.

[45] A summary of experimental results for ARM acquisition in magnetite samples is shown in Figure 13a. Particles with grain sizes <60 nm exhibit the d^2 dependence on grain size predicted by the model of this paper. A drastic change in the grain-size dependence of ARM occurs for $d > 60$ nm, as expected from micromagnetic calculations. Between 60 and 200 nm, the ARM intensity decreases as $d^{-0.8}$ with grain size d . In this grain-size range, the ARM may be controlled by thermal activations of nonuniform reversal modes. Above 200 nm (the upper limit for SD remanence), the ARM intensity depends weakly on grain size, and is related to a multidomain remanence. Experimental results for the median destructive field of SIRM and ARM are summarized in Figure 13b. The coercivity of small particles is reduced by the fluctuation field, and the observed trend for particles smaller than 100 nm is compatible with the result predicted by equation (41).

6. An Experimental Proof

[46] In this section, the theory of the ARM acquisition by noninteracting SD particles is verified experimentally on a

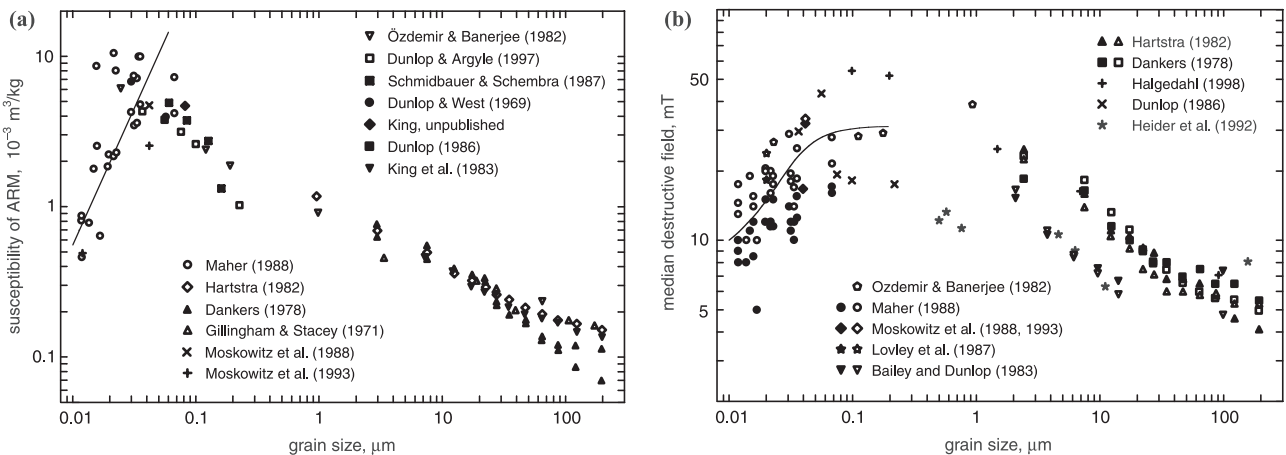


Figure 13. Summary of experimental results for ARM and IRM magnetizations in synthetic magnetite samples as a function of grain size. (a) Susceptibility of ARM. Data of *Schmidbauer and Schembra* [1987] are corrected to a magnetite concentration of $\sim 1\%$ according to the experimental dependence of the ARM on concentration reported by *Sugiura* [1979]. The solid line represents the quadratic dependence of the ARM on the grain size, predicted by the theory of this paper for SD particles. Experimental results are compatible with the theory for grain sizes up to 50 nm, close to the limit of 60 nm reported by *Enkin and Williams* [1994] for a magnetic moment reversal by coherent rotation. (b) Median destructive fields of SIRM (symbols in the left legend) and ARM (symbols in the right legend). The solid line represents the median destructive field calculated with the theory of this paper assuming a lognormal grain size distribution for each sample. The dispersion parameter of the lognormal distribution ($\sigma = 0.37$) is a best fit of the grain size distributions reported for the samples of *Maier* [1988].

sample from the Yucca Mountain Tuff [Worm and Jackson, 1999]. The Yucca Mountain Tuff is an ash flow tuff from the Tiva Canyon member of the Paintbrush Tuff at Yucca Mountain (Nevada). It contains small titanomagnetite grains with a narrow size distribution over the SP and finest SD range. The concentration of the magnetic grains is low (<0.5% by weight) and is not affected by clustering, so that magnetostatic interactions are expected to be small. The grains are Ti-poor titanomagnetites with a Curie temperature of 521°C, which corresponds to an ulvospinel content of $x = 0.1$. A room temperature saturation magnetization of 407 kA/m is assumed for the grains, according to Worm and Jackson [1999].

[47] Among the three samples mentioned by Worm and Jackson [1999], the more coarse-grained (CS914) is investigated here for its ARM properties. CS914 is the only sample with a significant amount of particles in the SD state at room temperature. According to electron microscopy and X-ray diffraction analysis, the grains have uniaxially prolate shapes with mean dimensions of 8.5×45 nm. The grains are much smaller than the upper limit for the SD state, and are therefore expected to switch by coherent rotation, with a microcoercivity of 221 mT. According to the properties illustrated above, the sample is therefore expected to behave as predicted by the model presented in this paper.

[48] The experimental proof is divided in two parts. In the first part, the dependence of the ARM intensity on the ramp rate of the AF field predicted by equation (32) is verified experimentally. The experiments allow a new estimation of the atomic reorganization time at room temperature. In the second part, the grain volumes distribution calculated by Worm and Jackson [1999] from thermal demagnetization curves is used to predict the ARM properties of the sample, which are then compared with the measurements.

6.1. Dependence of ARM Intensity on the Decay Rate of the AF Field

[49] The ARM model of this paper can be tested by investigating the predicted dependence of the ARM intensity on parameters which can be experimentally varied, like the temperature and the AF field decay rate. The product $f_{AC}\Delta\dot{H}$ in equation (32) is equivalent to half the decay rate α , expressed in T/s, which represents the drop of the AC peak field per unit time. The dependence on the decay rate is expected to be extremely weak, on the order of 30% when α changes over 3 orders of magnitude. The temperature dependence is stronger, however, its interpretation is difficult, because the intrinsic properties of the magnetic grains (e.g., saturation magnetization and microcoercivity) are temperature-dependent as well. In addition, in samples with a high proportion of SP particles, as is the case with the Yucca Mountain Tuff, an appreciable amount of particles becomes blocked or unblocked with little temperature change. For these reasons, the temperature dependence cannot be predicted with the necessary precision.

[50] The experimental verification of the dependence of the ARM intensity on the decay rate allows experimental evaluation of the atomic reorganization time, expressed by the frequency F_0 in equation (32). This estimation is important, since the atomic reorganization time depends on several experimental conditions, and the values given in the literature vary from 10^{-8} to 10^{-11} s [Brown, 1959; McNab et al., 1968].

[51] In order to measure the weak effect of the field decay rate, the widest range of decay rates made possible by the laboratory instrumentation was tested. Two types of demagnetization apparatus were used for this purpose: a GSD-1 Schoensted specimen demagnetizer with selectable nominal decay rates between 0.1 and 5 μ T/half cycle and an operating frequency of 400 Hz, and a custom-built 2G degausser system with selectable decay rates between 9 and 78 μ T/half cycle and an operating frequency of 150 Hz. The systems have overlapping decay rates from 0.059 to 24 mT/s, which cover 3 orders of magnitude. The 2G degausser system has a built-in facility for ARM acquisition. A supplementary coil was built around the Schoensted demagnetizer, in order to produce a DC field. The coil was connected to a high-precision current generator through an inductive filter, in order to avoid feedback effects with the demagnetization coil. Ramp rate, DC field, initial AF peak field and frequency were measured at each ARM acquisition. Because of the weak effect to be tested, extreme precision was required for the experiment. A comparison between the ARM acquisition with different ramp rates has to be performed at constant temperature. For this reason, special care was taken to avoid temperature changes during the acquisition process. The time required for the ARM acquisition at the lowest ramp rate (20 min) was long enough to transfer the Joule heat loss of the coil to the sample. For this reason, coil and sample were preheated with several AF cycles to achieve an equilibrium temperature before starting the acquisition. The temperature was controlled within $\pm 2^\circ\text{C}$, so that the related temperature effect was <0.5% of the total ARM. The ARM acquisitions were repeated 9 times for each decay rate, in order to increase the precision and estimate the experimental errors. The results are plotted in Figure 14.

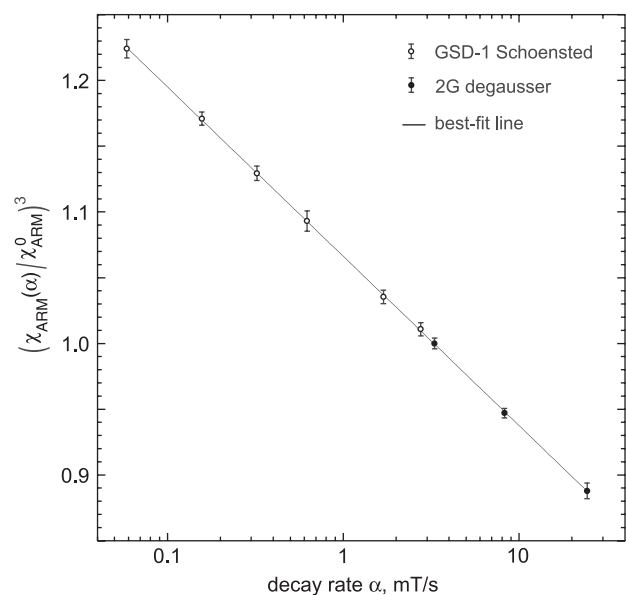


Figure 14. Dependence of the ARM intensity on the decay rate of the AF field for sample CS914. The error bars represent the double standard deviation of nine identical measurements for each point. The ARM intensity is normalized by its value for a decay rate of 3.31 mT/s, which is normally used in our laboratory.

[52] In order to linearize the dependence of χ_{ARM} on the decay rate α , equation (32) can be rewritten as follows:

$$\left(\frac{\chi_{\text{ARM}}(\alpha)}{\chi_{\text{ARM}}^0}\right)^q = a + b \log \alpha$$

$$q = 3; a = 1 + \frac{\ln \alpha_0}{\ln \left[\frac{0.7F_0}{\alpha_0 \sqrt{H_K}} \left(\frac{kT}{m}\right)^{3/2} \right]}; b = \frac{-\ln 10}{\ln \left[\frac{0.7F_0}{\alpha_0 \sqrt{H_K}} \left(\frac{kT}{m}\right)^{3/2} \right]} \quad (42)$$

whereby α_0 is a reference value of α and $\chi_{\text{ARM}}^0 = \chi_{\text{ARM}}(\alpha_0)$. A comparison of equation (42) with the experimental results allows verification of the expected linear relation and to estimate the constants a and b with least squares fitting. The linearity of (42) was tested by fitting the measurements of Figure 14 with different values of the exponent q . The effect of the measurement errors was simulated by adding an adequate Gaussian noise to each measurement. The result of 10,000 simulations gives $q = 3.11 \pm 0.12$, in good agreement with the theoretical value $q = 3$.

[53] The frequency F_0 can be estimated from equation (42):

$$F_0 = 1.44\alpha_0 \sqrt{H_K} 10^{1/b} \left(\frac{m}{kT}\right)^{3/2} \quad (43)$$

The mean values of m and H_K for the Yucca Mountain Tuff can be deduced from *Worm and Jackson* [1999]: $m = 2.1 \times 10^{-18}$ A m² and $H_K = 220$ mT. They were taken as starting values of equation (43). From Figure 14, $\alpha_0 = 3.31$ mT/s and $b = 0.129 \pm 0.00002$. A better estimation of m and H_K can be obtained with the AF demagnetization curve of ARM discussed in section 6.2 and shown in Figure 16b. Equation (32) can be solved with respect to m , obtaining

$$m = kT \sqrt{H_K} \left(\frac{\chi_{\text{ARM}}}{1.797 \mu_0 M_{\text{rs}}} \right)^{3/2} \ln^{-1/2} \left[\frac{0.696 F_0}{\alpha} \left(\frac{kT}{m} \right)^{3/2} \right] \quad (44)$$

As first estimation, $H_K = 1.91(\tilde{H}_{1/2} + H_q)$ was chosen, with $\tilde{H}_{1/2}$ being the median destructive field of the AF demagnetization curve of ARM. Equations (41), (43), and (44) were then iteratively evaluated in order to get better estimates of m and H_K . The final values obtained are $m = (2.8 \pm 0.7) \times 10^{-18}$ A m² and $H_K = 184 \pm 40$ mT, in good agreement with the initial values taken from *Worm and Jackson* [1999]. Finally, equation (43) gives the following estimate: $F_0 = (1.3 \pm 0.4)$ GHz or $\tau_0 = (7.7 \pm 2) \times 10^{-10}$ s, in good agreement with the values found in the literature. *McNab et al.* [1968] estimated $\tau_0 = (9.5 \pm 1.5) \times 10^{-10}$ s for superparamagnetic magnetite grains using Mössbauer spectra, which is compatible with the result of this paper within the error range. For comparison, *Worm and Jackson* [1999] estimated $F_0 \approx 10^9$ – 10^{11} Hz by modeling the frequency dependence of the susceptibility on the same sample. Their lower estimation limit of $F_0 \approx 10^9$ fits better the measured susceptibility at low frequencies (0.1–1 Hz), which is controlled mainly by relatively stable particles with time constants of 1–10 s. These particles are only slightly smaller than the stable SD particles which are contributing to the ARM. The reason for the apparent dependence of F_0 on the particles size in CS914 is not clear: it is maybe due to

the difficulty of modeling the susceptibility of particles near the SP/SD boundary.

6.2. A Comparison Between Calculated and Measured ARM Properties

[54] In section 3, a relation between the microscopic properties of fine particles (magnetic moment and microcoercivity) and ARM was found. The Yucca Mountain Tuff is a suitable material for testing this relation, since size, shape and mineralogy of the magnetic grains is well known.

[55] Knowledge of the distribution of volumes and microcoercivities of the grains (magnetic granulometry [*Dunlop*, 1976]) allows us to predict their magnetic properties, including the ARM. In this section, the magnetic granulometry will be deduced from IRM experiments. The results will be then used to calculate the ARM properties with equations (32), (33), and (41), which are then compared with the ARM measurements.

[56] *Worm and Jackson* [1999] calculated the volume distribution of the magnetic particles in sample CS914 using thermal demagnetization curves of IRM. Their result is shown in Figure 15a for volumes up to 6×10^{-24} m³. The shape of the volume distribution suggests the presence of larger particles. In order to extrapolate the contribution of larger volumes, the distribution was fitted in the SD region ($V > 2 \times 10^{-24}$ m³) with two lognormal functions. Since the measurements of this paper are performed at room temperature, a misfit below the SP/SD boundary is irrelevant. The extrapolated distribution suggests significant amounts of particles with volumes up to 8×10^{-24} m³. Assuming a mean microcoercivity of 220 mT from microscopic observations of the grain shapes, and with equation (41), the coercivity of the particles is expected to range from 0 to 110 mT. This broad coercivity distribution is controlled by the strong dependence of the fluctuation field on the volume of fine SD particles. It is reasonable to assume some kind of variations in the grain shape, which is related to a distribution of microcoercivities around 220 mT. This distribution can be deduced from the volume distribution and from the coercivity distribution calculated with IRM acquisition or demagnetization curves. Let $N(H_K, V)$ and $M'(H_{\text{sw}})$ be the distributions of H_K , V , and the switching field H_{sw} , respectively. Further, $H_{\text{sw}} = 0.524H_K - H_q(H_K, V)$, as discussed in section 4. The distribution $N(H_K, V)$ was called magnetic granulometry by *Dunlop* [1976]. The relation between magnetic granulometry and coercivity distribution is then given approximately by

$$M'(H_{\text{sw}}) = \int_0^\infty \frac{N(H_K, V)}{0.524 - dH_q/dH_K} M_s V dV \quad (45)$$

Except the SP/SD boundary, $dH_q/dH_K \ll 1$, and equation (45) reduces to

$$M'(H_{\text{sw}}) \cong 1.91 M_s \int_0^\infty N(H_K, V) V dV \quad (46)$$

The AF demagnetization curve of SIRM is shown in Figure 16a, the related coercivity distribution $M'(H_{\text{sw}})$ is given by the first derivative. In order to solve (45), $N(H_K, V)$ is assumed to be the sum of two distributions, which are

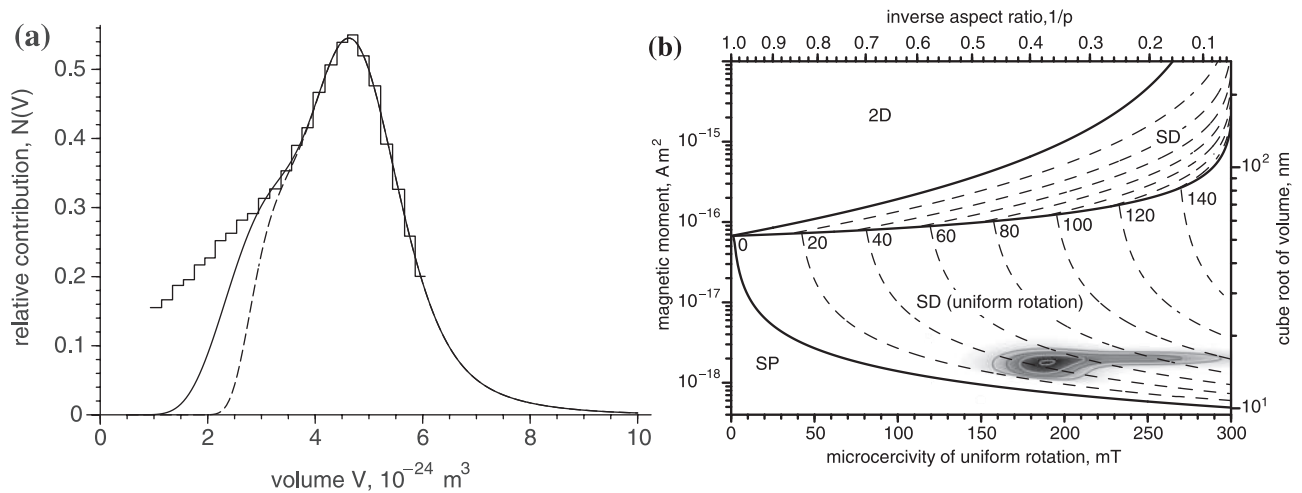


Figure 15. (a) Volumes distribution of the magnetite particles in sample CS914. The stepped line is the volume distribution calculated from the thermal demagnetization of IRM (from *Worm and Jackson* [1999]). The solid line is a best fit of the volume distribution in the SD range ($V > 2.5 \times 10^{-24} \text{ m}^3$) with two lognormal distributions. The dashed line is the volume distribution of all particles that can carry a remanence at room temperature. (b) Distribution of volumes and microcoercivities in sample CS914 (contours and shaded surface), plotted together with the stability range for SD particles. This distribution gives a best fit to both thermal and AF demagnetization curves of SIRM. The density of the distribution is proportional to the contribution of all particles with given volume and microcoercivity to the SIRM. The dashed lines in the SD range represent all particles with the same coercivity, indicated by the numbers in the plot field. A typical coercivity of 45 mT can be deduced from the plot: this value coincides with the median destructive field of the AF demagnetization.

expressed with lognormal functions of V , and Gaussian functions of H_K . The parameters of the functions were varied until the best agreement with the volume distributions of *Worm and Jackson* [1999] and with $M'(H_{sw})$ was reached. The resulting magnetic granulometry is plotted in Figure 15b, together with the SD boundaries calculated in section 5. The mean values of volume and microcoercivity are $\bar{V} = 4.3 \times 10^{-24}$ and $\bar{H}_K = 190$ mT, in good agreement with *Worm and Jackson* [1999]. From Figure 15b, a typical coercivity of

40 mT can be deduced, and this value corresponds to the median destructive field of the AF demagnetization curve of Figure 16a. Notice that ARM properties were not used to estimate the magnetic granulometry.

[57] In order to calculate the ARM properties for sample CS914, an artificial set of 50,000 particles was created according to the magnetic granulometry of Figure 15. With this set of particles, AF demagnetization curves of SIRM and ARM were calculated assuming a negligible degree of

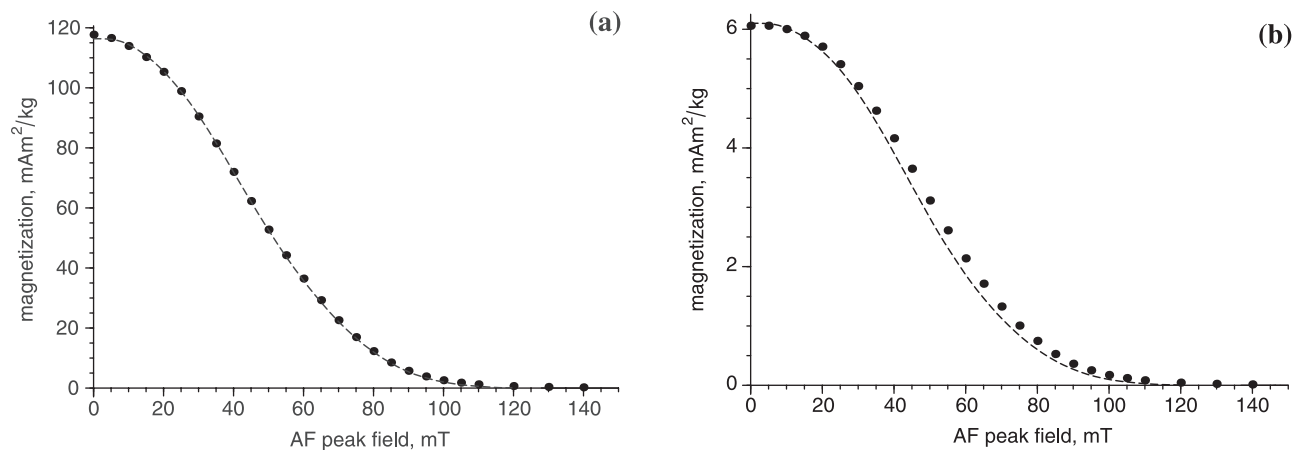


Figure 16. Comparison between measured and modeled AF demagnetization curves of SIRM and of ARM, both for sample CS914. The modeled curves are calculated from the distribution of volumes and microcoercivities of Figure 15b. (a) AF demagnetization of room temperature SIRM. Dots are measured points; the dashed line is the model. (b) AF demagnetization curve of room temperature ARM (0.1 mT DC field, 300 mT AF peak field). Dots are measured points; the dashed line is the model. Both curves have similar shape and identical amplitude. This agreement is excellent, considering that the magnetic properties of the particles were deduced only from IRM measurements.

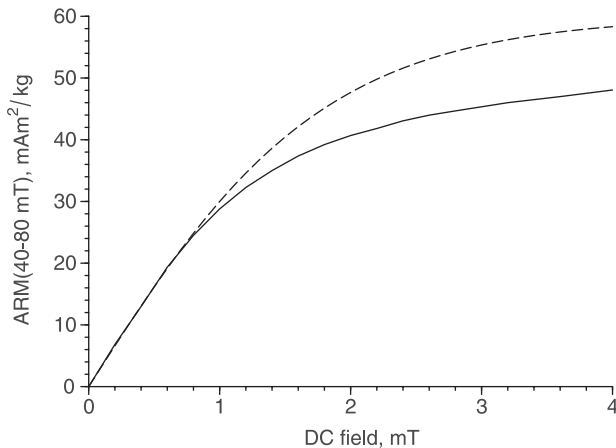


Figure 17. ARM intensity of sample CS914 as a function of the DC field. The sample was given an ARM with 80 mT AF peak field, and subsequently, it was demagnetized with 40 mT AF peak field in order to measure the magnetization of all particles with coercivities between 40 and 80 mT. The ARM model of this paper assumes the DC field to be much smaller than the coercivity of the particles. Since DC fields up to 4 mT are necessary to approach saturation, the 40 mT AF demagnetization will allow us to compare the measurements (solid line) with the modeled curve (dashed line). The ARM model is able to predict the value of the ARM susceptibility within an error of 1%. Disagreement between model and measurements in the saturation range, for DC fields >1 mT, may be due to interaction effects.

magnetic interactions. The ARM curve was calculated using equation (32) with the atomic reorganization frequency estimated in section 6.1. The calculated demagnetization curve of ARM is in excellent agreement with the measurements (Figure 16b), both in intensity and shape. The calculated ARM intensity differs only by 1% from the measured value. Differences between modeled and measured coercivity distributions of ARM are within 10% over all the coercivity range.

[58] Furthermore, the dependence of the ARM on the DC-field predicted by equation (33) was also calculated with the magnetic granulometry assumed in Figure 15. Considering the small grain sizes, saturation of ARM is expected to occur at relatively high values of the DC field. An ARM with 80 mT AC peak field and different DC field values up to 4 mT was given to the sample. Since the ARM model discussed in section 3 assumes $H_{DC} \ll H_K$, the magnetization of the particles that do not satisfy this condition was removed with a 40 mT AF demagnetization. The results are shown in Figure 17. The initial part of the acquisition curve is controlled only by the susceptibility of ARM, and is in excellent agreement with the model of this paper. A disagreement is found in the range of saturation, above 1 mT. This may be due to interaction effects.

7. Interpretation of the Modified Lowrie-Fuller Test for SD Particles

[59] Experiments based on ARM and IRM acquisition and their demagnetization curves are commonly used as an indicator for the domain state of the particles. In the original

Lowrie-Fuller test [Lowrie and Fuller, 1971] a comparison of normalized AF demagnetization curves of TRM and SIRM was used to distinguish between SD and MD grains. For multidomain carriers of remanence, saturation IRM is relatively more stable than weak-field TRM; for single domain carriers, the opposite is true. Soon after the test was proposed, Schmidt [1976] predicted that MD grains could pass the SD criterion and vice versa. Later, the more easily produced ARM was substituted for TRM, and a modified Lowrie-Fuller test based on ARM characteristics was proposed [Johnson et al., 1975]. Newell [2000] calculated that the Lowrie-Fuller test for SD particles can give opposite results, depending on such particle properties as volume and coercivity. A similar result for the ARM is shown in this section. Also, cases of MD particles which show SD-type behavior are reported in the literature [Hartstra, 1982; Bailey and Dunlop, 1983; Heider et al., 1992]. Xu and Dunlop [1995] modeled the result of the Lowrie-Fuller test for MD particles and came to the conclusion that the Lowrie-Fuller test is sensitive not only to the grain size of the particles: other factors like the density of dislocations in the crystals and the microcoercivity distribution are also important. They therefore replaced the confusing terms “SD-type” by “L-type” (low-field remanence is more stable), and “MD-type” by “H-type” (high-field remanence is more stable).

[60] Results of the modified Lowrie-Fuller test for a set of identical, randomly oriented and noninteracting SD particles are shown in Figure 18. The shapes of the normalized demagnetization curves of ARM and IRM are practically identical. According to the classical interpretation of the Lowrie-Fuller test, the small differences in the shapes of the demagnetization curves are characteristic for SD particles only if their volume is very close to the SP boundary. Significant and systematic differences in the shape of the demagnetization curves cannot arise from a set of identical, noninteracting SD particles. The result of the modified Lowrie-Fuller test for SD particles is therefore not related to their intrinsic magnetic properties.

[61] Significant differences in the shape of normalized AF demagnetization curves of ARM and IRM can be produced with a combination of different populations of SD particles. Results of the modified Lowrie-Fuller test obtained from synthetic sets of noninteracting SD particles with different volumes and microcoercivities are shown in Figure 19. In general, the result of the modified Lowrie-Fuller test depends on the statistical relation between the volume and the coercivity distribution of the particles. If the volume and the coercivity distribution are statistically uncorrelated, the normalized demagnetization curves of ARM and IRM do not differ systematically. In case of a positive correlation between the two distributions, the size of the particles increases as the coercivity increases. Since the ARM to IRM ratio depends mainly on the volume of the particles, large particles acquire a relatively strong ARM, and the related demagnetization curve is steeper at large coercivities and flatter at small coercivities, if compared to the demagnetization of IRM. Consequently, the normalized demagnetization curve of ARM lies above the demagnetization curve of IRM. In other words, the ARM is apparently more resistant against demagnetization than IRM, and the modified Lowrie-Fuller test is positive for SD particles. On the other hand, in the case of a negative correlation

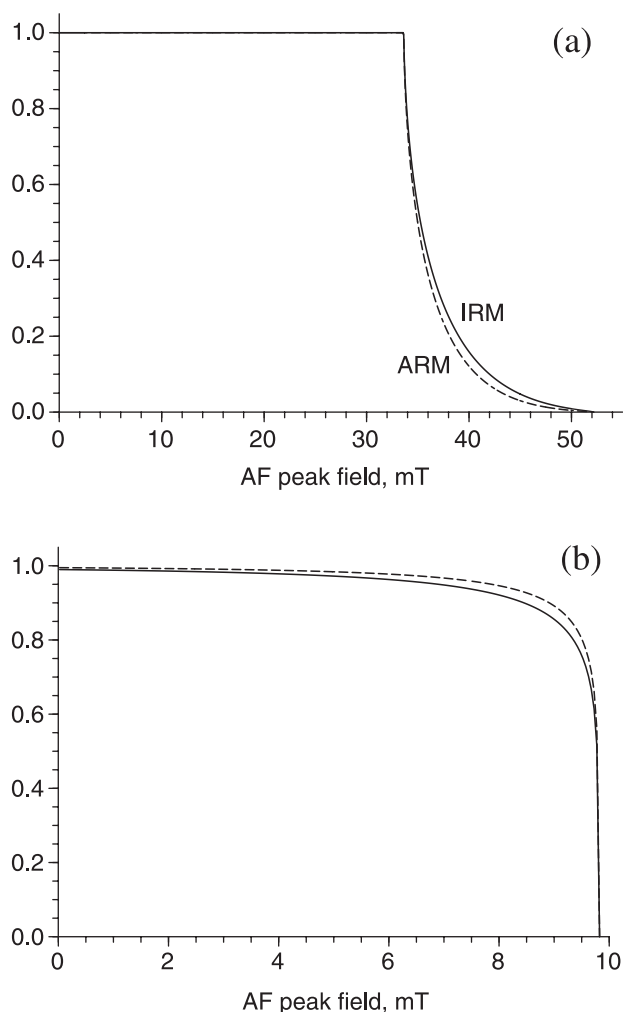


Figure 18. Normalized AF demagnetization curves of ARM (dashed lines) and IRM (solid lines) for a set of identical, randomly oriented and non-interacting SD particles with $\mu_0 H_K = 80$ mT. Particles with a moment of (a) 2×10^{-17} A m² and (b) 2.4×10^{-18} A m² show opposite relative stabilities of ARM and IRM in the modified Lowrie-Fuller test, although both sets are SD particles.

between the volume and the coercivity distribution, the opposite situation occurs, and the ARM is apparently less resistant against demagnetization than IRM. The result of the modified Lowrie-Fuller test would indicate the presence of multidomain particles. Mixed situations where the two demagnetization curves cross each other are also possible.

[62] From the considerations above, it seems that the result of the modified Lowrie-Fuller test for SD particles can be either negative or positive, depending on their volume and coercivity distributions. On the other hand, many experimental observations [Dunlop and West, 1969; Johnson et al., 1975] suggest that the result of the modified Lowrie-Fuller test is generally consistent with the domain state of the particles. This consistence can be explained if a positive correlation between the volume and the coercivity distribution is assumed to be a typical feature of SD particles. Figure 20 shows how this correlation can be

generated with no assumption about the intrinsic magnetic properties of the particles other than a mean value for the distribution of volumes and microcoercivities. First, an artificial set of 100,000 particles was generated. The volume and the axial ratio of the particles were chosen to be lognormally distributed and uncorrelated. The resulting microcoercivity distribution is also not correlated to the volumes. Consider now two particles with identical shape (microcoercivity) and different volumes. The smaller particle has a larger fluctuation field and consequently a smaller coercivity. In this way, volumes and coercivities of a random set of particles are positively correlated, and the modified Lowrie-Fuller test is positive for SD particles, as shown in Figure 20c. The shape difference between the normalized demagnetization curves of ARM and IRM increases with the amount of dispersion of the volume distribution: particles with similar volumes produce demagnetization curves of ARM and IRM with similar shape.

[63] Magnetic interaction effects can also produce systematic differences between the normalized demagnetization curves of ARM and IRM. Interaction models based on the Preisach-Néel theory predict that the ARM acquisition of particles with a small coercivity is reduced by the interaction field produced by the particles with large coercivity [Wohlfarth, 1964]. This process is equivalent to a volume reduction by an amount which increases as the coercivity decreases or, in other words, to a positive correlation between volumes and coercivities. Therefore magnetic interactions apparently increase the relative resistance of ARM against demagnetization. The modified Lowrie-Fuller test is also affected by the fact that the size at which the coercivity of a SD grain is maximum differs from the maximum size a grain can be uniformly magnetized in zero field [Newell and Merrill, 1999].

[64] To conclude, a relation between the result of the modified Lowrie-Fuller test and the domain state of the particles does not necessarily exist. Shape differences between the normalized demagnetization curves of ARM and IRM are related to the statistical distribution of the intrinsic magnetic properties of the particles and not to the properties themselves. Some volume and microcoercivity distributions of SD particles can produce H-type properties. On the other hand, a random distribution of well-dispersed volumes and microcoercivities in the SD range is always of L-type. Therefore, the modified Lowrie-Fuller test is effective in the identification of one population of SD particles, but can fail with special combinations of two or more populations of SD particles. Figure 21 summarizes various results of the modified Lowrie-Fuller test as a function of the grain size. The result of the test is represented by the parameter MDF_{ARM}/MDF_{SIRM} , which is the ratio between the median destructive fields of ARM and SIRM. A general trend toward the classical interpretation of the test is evident: all SD samples are of L-type. On the other hand, the majority but not all MD samples are of H-type. The SD samples have highly scattered values of MDF_{ARM}/MDF_{SIRM} , although they all contain a single population of particles. The theory of this paper predicts values slightly larger than 1 for those samples. The observed scattering is probably due to magnetic interaction effects: samples with virtually no interactions (CS914 in this paper and Moskowitz et al. [1988]) have MDF ratios between 1 and 1.1, whereas the others can

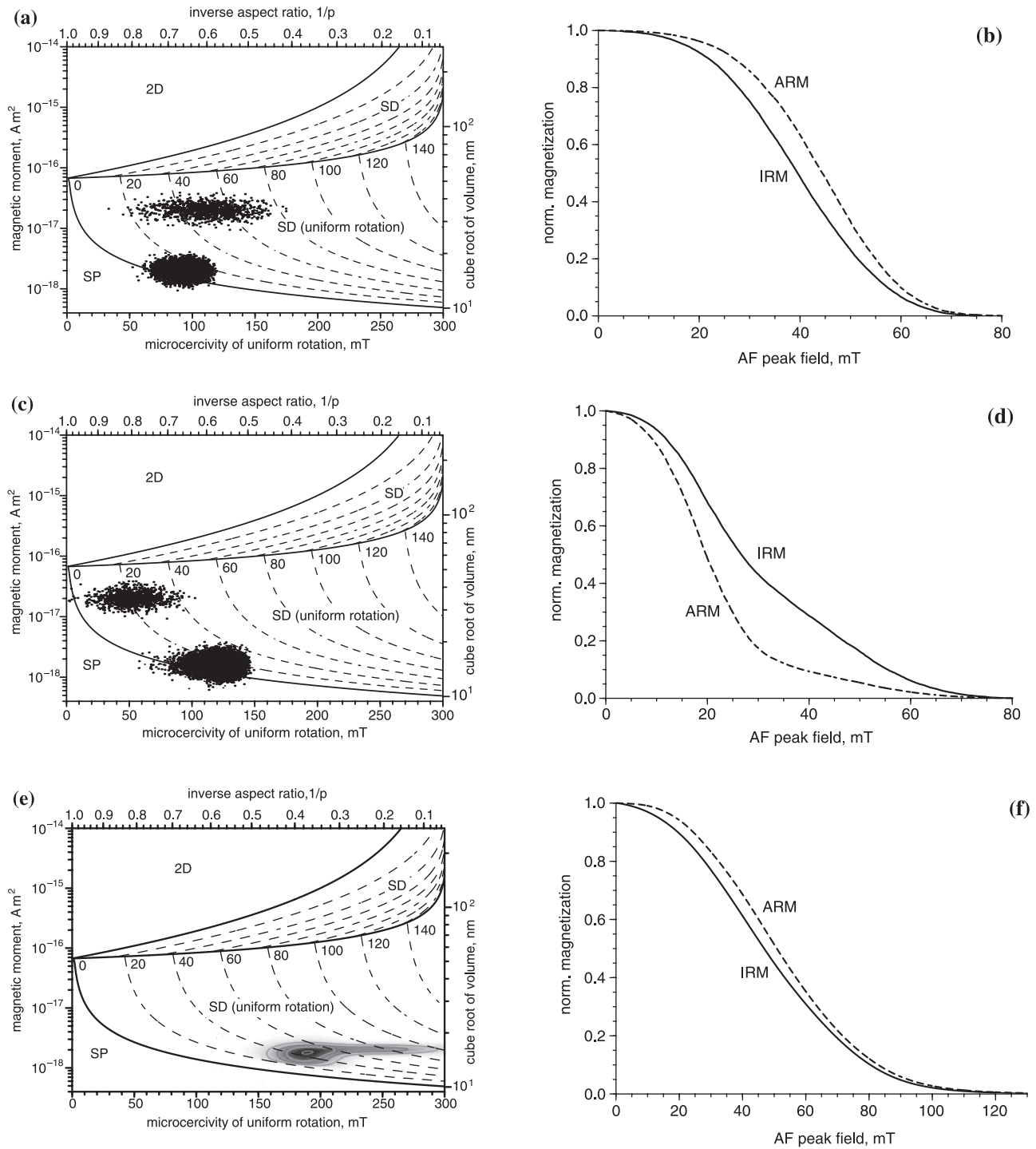


Figure 19. Results of the modified Lowrie-Fuller test for three sets of 12,000 noninteracting SD particles with different volumes (right axis) and microcoercivities (left axis). Each point in the left plots indicates the volume and the microcoercivity of a single particle. The sum of the two particle populations in Figure 19a gives a positive test for SD particles, plotted in Figure 19b. The opposite result is obtained in Figure 19d with another combination of SD particles, plotted in Figure 19c. For comparison, the result of the modified Lowrie-Fuller test for sample CS914 is plotted in Figure 19f. The corresponding volume and microcoercivity distribution are plotted in Figure 19e.

reach MDF ratios up to 2.2. An increase of the MDF ratio due to interaction effects is predicted by the Preisach-Néel theory.

[65] A conclusive statement about the result of the Lowrie-Fuller test for small SD particles is the following: (1) SD

particles with a random distribution of volumes and microcoercivities have an L-type behavior, which is eventually enhanced by magnetic interactions and (2) samples that contain different populations of SD particles with a suffi-

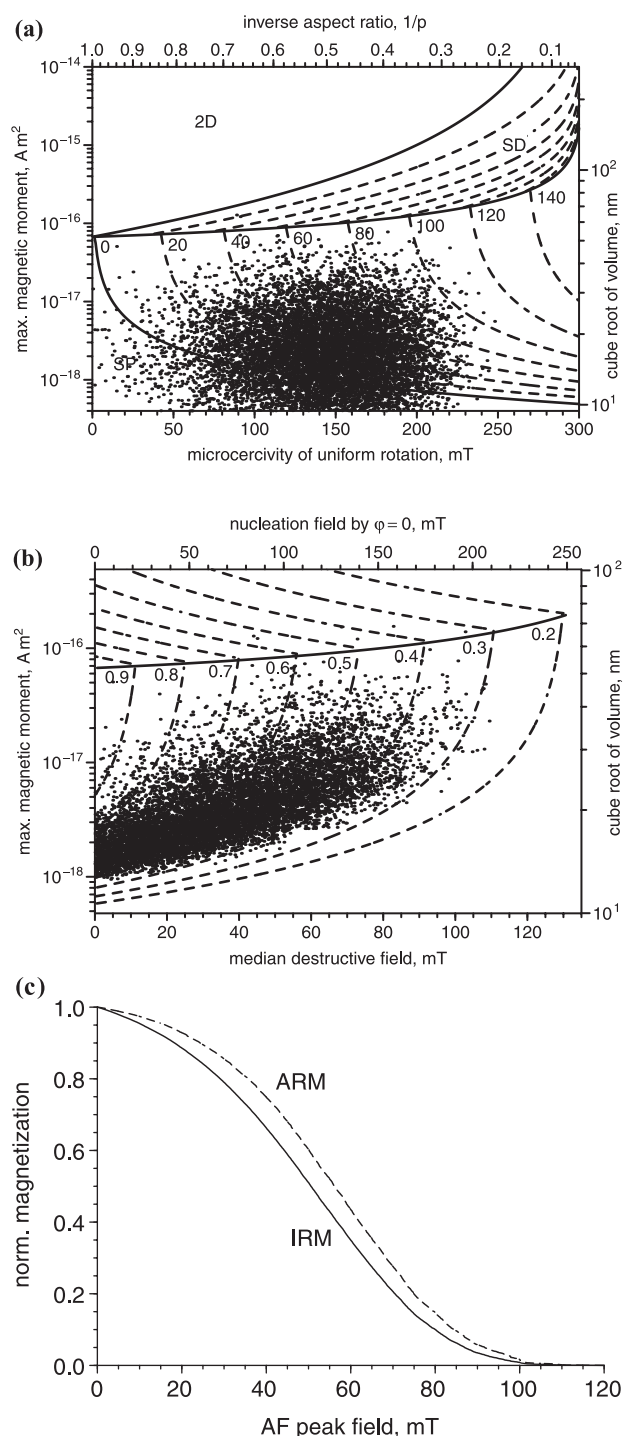


Figure 20. Result of the modified Lowrie-Fuller test for a set of 100,000 noninteracting SD particles. The axial ratio and the volume of the particles were chosen to be lognormal distributed and uncorrelated. (a) Magnetic moment and microcoercivity of a random selection of 10,000 particles (points) among the 100,000 calculated. (b) Magnetic moment and median destructive field for the same selection of particles as in Figure 20a. Because of the volume dependence of the fluctuation field, the magnetic moment and the median destructive field are correlated. (c) Normalized AF demagnetization curves of ARM (dashed line) and IRM (solid line) calculated for the entire set of 100,000 particles.

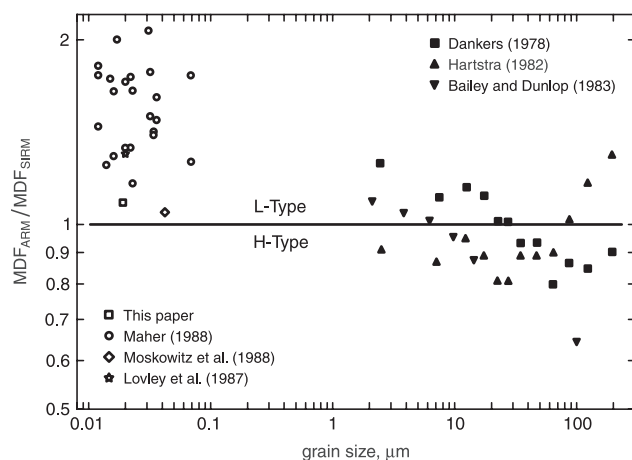


Figure 21. Summary of experimental results of the modified Lowrie-Fuller test in synthetic and natural magnetite samples as a function of the grain size. On the vertical axis, the ratio between the median destructive fields of ARM and SIRM is shown. Values >1 of this ratio denote a L-type behavior (see text), which is considered typical for SD particles. The opposite is true for a H-type behavior. Not all MD particles are characterized a H-type behavior.

ciently high negative correlation between volumes and microcoercivities can show an H-type behavior.

8. Conclusions

[66] The ARM acquisition process in small noninteracting SD particles can be explained in terms of thermal activation processes. Equations (32) and (33) describe the dependence of ARM on the properties of the particles. The ARM intensity depends on the grain size ($\propto d^2$), the microcoercivity ($\propto H_K^{-1/3}$), the temperature ($\propto T^{-2/3}$) and weakly on the ramp rate α of the alternating magnetic field ($\propto \ln^{1/3}(10^4 \alpha^{-1})$). These dependences are valid in a range where the grains switch their moment by coherent rotation. Other reversal modes occur in grains larger than 60 nm. Various ARM measurements performed by different authors confirm the d^2 dependence of the ARM for $d < 60$ nm. For larger grain sizes up to the upper limit for SD remanence, the thermal activation model discussed in this paper may still be valid, but microcoercivities and energy barriers have to be recalculated for the case of nonuniform moment switching. A decrease of the ARM intensity with grain size is expected over 60 nm.

[67] The thermal activation model presented in this paper allowed also a new estimation of the fluctuation field, given in equation (41), and consequently also of the coercivity of SD grains. The model was tested with a natural sample of well-dispersed acicular magnetite grains. Precise ARM measurements confirmed the results predicted by equations (32) and (33) within an error of 1%. Measurements of the dependence of the ARM intensity on the AF field decay rate allowed a precise estimation of the atomic reorganization time, in agreement with values given by McNab *et al.* [1968].

[68] This paper demonstrates that ARM of well-dispersed fine SD particles is controlled by intrinsic properties such as grain size and shape. Magnetic interactions are not necessary to explain the ARM acquisition process of SD grains.

However, as shown by different authors, interactions can play a dominant role in samples with a high concentration of clustered grains, as likely occur in some natural rocks and in many artificial samples. The ARM/SIRM ratio can therefore be a useful parameter for the characterization and identification of populations of well-dispersed magnetic particles over the entire range of grain sizes.

[69] It has also been shown that the modified Lowrie-Fuller test for small noninteracting SD particles does not depend on their intrinsic properties, and can give contradictory results. However, the calculated result of the modified Lowrie-Fuller test for a random distribution of volumes and microcoercivities is compatible with the results reported by Johnson *et al.* [1975].

[70] **Acknowledgments.** We have benefited from useful discussions with Luca Lanci about the origin of ARM in SD particles. Horst-Ulrich Worm kindly provided us with sample CS914. We are grateful to Andrew Newell for an informal review of section 3 and to Ron Merrill and an anonymous reviewer for their constructive comments. ETH Research Project 0-20556-00.

References

- Aharoni, A., Thermal agitation of single domain particles, *Phys. Rev. A*, **135**, 447–449, 1964.
- Aharoni, A., and S. Shtrikman, Magnetization curve of the infinite cylinder, *Phys. Rev.*, **109**, 1522–1528, 1958.
- Bailey, M. E., and D. J. Dunlop, On the use of anhysteretic remanent magnetization in paleointensity determination, *Phys. Earth Planet. Inter.*, **13**, 360–362, 1977.
- Bailey, M. E., and D. J. Dunlop, Alternating field characteristics of pseudo-single-domain (2–14 μm) and multidomain magnetite, *Earth Planet. Sci. Lett.*, **63**, 335–352, 1983.
- Banerjee, S. K., and J. P. Mellema, A new method for the determination of paleointensity from the ARM properties of rocks, *Earth Planet. Sci. Lett.*, **23**, 177–184, 1974.
- Brown, W. F., Relaxation behavior of fine particles, *J. Appl. Phys.*, **30**, 1305–1325, 1959.
- Brown, W. F., Thermal fluctuation of a single-domain particle, *Phys. Rev.*, **130**, 1677–1686, 1963.
- Butler, R. F., and S. K. Banerjee, Theoretical single-domain grain size range in magnetite and titanomagnetite, *J. Geophys. Res.*, **80**, 4049–4058, 1975.
- Dankers, P. H. M., Magnetic properties of dispersed natural iron-oxides of known grain-size, Ph.D. thesis, Univ. of Utrecht, Utrecht, Netherlands, 1978.
- Diaz Ricci, J. C., and J. L. Kirschvink, Magnetic domain state and coercivity predictions for biogenic greigite (Fe_3S_4): A comparison of theory with magnetosome observations, *J. Geophys. Res.*, **97**, 17,309–17,315, 1992.
- Dunlop, D. J., Grain distributions in rocks containing single-domain grains, *J. Geomagn. Geoelectr.*, **17**, 459–471, 1965.
- Dunlop, D. J., Thermal fluctuation analysis: A new technique in rock magnetism, *J. Geophys. Res.*, **81**, 3511–3517, 1976.
- Dunlop, D. J., The rock magnetism of fine particles, *Phys. Earth Planet. Inter.*, **26**, 1–26, 1981.
- Dunlop, D. J., Coercive forces and coercivity spectra of submicron magnetites, *Earth Planet. Sci. Lett.*, **78**, 288–295, 1986.
- Dunlop, D. J., and K. S. Argyle, Thermoremanence, anhysteretic remanence and susceptibility of submicron magnetites: Nonlinear field dependence and variation with grain size, *J. Geophys. Res.*, **102**, 20,199–20,210, 1997.
- Dunlop, D. J., and Ö. Özdemir, *Rock Magnetism*, Cambridge Univ. Press, New York, 1997.
- Dunlop, D. J., and G. West, An experimental evaluation of single-domain theories, *Rev. Geophys.*, **7**, 709–757, 1969.
- Eldridge, D. F., Quantitative determination of the interaction fields in aggregates of single-domain particles, *J. Appl. Phys.*, **32**, 247S–249S, 1961.
- Enkin, R. J., and W. Williams, Three-dimensional micromagnetic analysis of stability in fine magnetic grains, *J. Geophys. Res.*, **99**, 611–618, 1994.
- Gillingham, E. W., and F. D. Stacey, Anhysteretic remanent magnetization (ARM) in magnetite grains, *Pure Appl. Geophys.*, **91**, 160–165, 1971.
- Halgedahl, S. L., Revisiting the Lowrie-Fuller test: Alternating field demagnetization characteristics of single-domain through multidomain glass-ceramic magnetite, *Earth Planet. Sci. Lett.*, **160**, 257–271, 1998.
- Halgedahl, S. L., and M. Fuller, Magnetic domain observations of nucleation processes in fine particles of intermediate titanomagnetite, *Nature*, **288**, 70–72, 1980.
- Hartstra, R. L., A comparative study of the ARM and I_{sr} of some natural magnetites of MD and PSD grain size, *Geophys. J. R. Astron. Soc.*, **71**, 497–518, 1982.
- Heider, F., D. J. Dunlop, and H. C. Soffel, Low-temperature and alternating field demagnetization of saturation remanence and thermoremanence in magnetite grains (0.037 μm to 5 mm), *J. Geophys. Res.*, **97**, 9371–9381, 1992.
- Jaep, W. F., Anhysteretic magnetization of an assembly of single-domain particles, *J. Appl. Phys.*, **40**, 1297–1298, 1969.
- Jaep, W. F., Role of interactions in magnetic tapes, *J. Appl. Phys.*, **42**, 2790–2794, 1971.
- Johnson, H. P., W. Lowrie, and D. Kent, Stability of anhysteretic remanent magnetization in fine and coarse magnetite and maghemite particles, *Geophys. J. R. Astron. Soc.*, **41**, 1–10, 1975.
- King, J. W., S. K. Banerjee, and J. Marvin, A new rock-magnetic approach to selecting sediments for geomagnetic paleointensity studies: Application to paleointensity for the last 4000 years, *J. Geophys. Res.*, **88**, 5911–5921, 1983.
- Kneller, E., Magnetic-interaction effects in fine-particle assemblies and thin films, *J. Appl. Phys.*, **39**, 945–955, 1968.
- Kneller, E., and E. P. Wolfarth, Effect of thermal fluctuations on the anhysteretic process in ferromagnetic fine-particle assemblies, *J. Appl. Phys.*, **37**, 4816–4818, 1966.
- Lovley, D. R., et al., Anaerobic production of magnetite by a dissimilatory iron-reducing microorganism, *Nature*, **330**, 252–254, 1987.
- Lowrie, W., and M. Fuller, On the alternating field demagnetization characteristics of multidomain thermoremanent magnetization in magnetite, *J. Geophys. Res.*, **76**, 6339–6349, 1971.
- Maher, B. A., Magnetic properties of some synthetic sub-micron magnetites, *Geophys. J.*, **94**, 83–96, 1988.
- McNab, T. K., R. A. Fox, and J. F. Boyle, Some magnetic properties of magnetite (Fe_3O_4) microcrystals, *J. Appl. Phys.*, **39**, 5703–5711, 1968.
- Moskowitz, B. M., et al., Magnetic properties of magnetotactic bacteria, *J. Magn. Magn. Mater.*, **73**, 273–288, 1988.
- Moskowitz, B. M., R. Frankel, and D. Bazylinski, Rock magnetic criteria for the detection of biogenic magnetite, *Earth Planet. Sci. Lett.*, **120**, 283–300, 1993.
- Néel, L., Théorie du trainage magnétique des ferromagnétiques en grains fins avec applications aux terres cuites, *Ann. Geophys.*, **5**, 99–136, 1949.
- Néel, L., Remarques sur la théorie des propriétés magnétiques des substances dures, *Appl. Sci. Res.*, **4**, 13–24, 1954.
- Néel, L., Some theoretical aspects of rock magnetism, *Adv. Phys.*, **4**, 191–243, 1955.
- Newell, A. J., The Lowrie-Fuller test: Single-domain and micromagnetic theory, *Earth Planet. Sci. Lett.*, **183**, 335–346, 2000.
- Newell, A. J., and R. T. Merrill, Single-domain critical sizes for coercivity and remanence, *J. Geophys. Res.*, **104**, 617–628, 1999.
- Özdemir, Ö., and S. K. Banerjee, A preliminary magnetic study of soil samples from west-central Minnesota, *Earth Planet. Sci. Lett.*, **59**, 393–403, 1982.
- Schmidbauer, E., and N. Schembra, Magnetic hysteresis properties and anhysteretic remanent magnetization of spherical Fe_3O_4 particles in the grain size range 60–160 nm, *Phys. Earth Planet. Inter.*, **46**, 77–83, 1987.
- Schmidt, V. A., The variation of the blocking temperature in models of thermoremanence (TRM), *Earth Planet. Sci. Lett.*, **29**, 146–154, 1976.
- Stoner, E. C., and E. P. Wohlfarth, A mechanism of magnetic hysteresis in heterogeneous alloys, *Philos. Trans. R. Soc. London*, **240**, 599–602, 1948.
- Sugiura, N., ARM, TRM, and magnetic interactions: concentration dependence, *Earth Planet. Sci. Lett.*, **42**, 451–455, 1979.
- Victoria, R. H., Predicted time dependence of the switching field for magnetic materials, *Phys. Rev. Lett.*, **63**, 457–460, 1989.
- Walton, D., A theory of anhysteretic remanent magnetization of single-domain grains, *J. Magn. Magn. Mater.*, **87**, 369–374, 1990.
- Wohlfarth, E. P., A review of the problem of fine-particle interactions with special reference to magnetic recording, *J. Appl. Phys.*, **35**, 783–790, 1964.
- Worm, H.-U., and M. Jackson, The superparamagnetism of Yucca Mountain Tuff, *J. Geophys. Res.*, **104**, 25,415–25,425, 1999.
- Xu, S., and D. J. Dunlop, Toward a better understanding of the Lowrie-Fuller test, *J. Geophys. Res.*, **100**, 22,533–22,542, 1995.
- Yamazaki, T., and N. Ioka, Cautionary note on magnetic grain-size estimation using the ratio of ARM to magnetic susceptibility, *Geophys. Res. Lett.*, **24**, 751–754, 1997.